Article

# New finds shed light on diet and locomotion in *Australopithecus deyiremeda*

https://doi.org/10.1038/s41586-025-09714-4

Received: 14 September 2024

Accepted: 6 October 2025

Published online: 26 November 2025

Open access

Check for updates

Yohannes Haile-Selassie[1]✉, Gary T. Schwartz[1], Thomas C. Prang[2], Beverly Z. Saylor[3], Alan Deino[4], Luis Gibert[5], Anna Ragni[6] & Naomi E. Levin[7]

The naming of *Australopithecus deyiremeda*[1] from Woranso-Mille (less than 3.59 to more than 3.33 million years) indicated the presence of a species contemporaneous with *Australopithecus afarensis* in the Ethiopian Afar Rift. A partial foot (BRT-VP-2/73)[2] and several isolated teeth from two Burtele (BRT) localities, however, were not identified to the species level. Recently recovered dentognathic specimens clarify not only the taxonomic affinity of the BRT hominin specimens but also shed light on the diet and locomotion of *A. deyiremeda*. Here we present a comparative description of these specimens and show that they are attributable to *A. deyiremeda*. We also find it parsimonious to attribute the BRT foot to this species based on the absence of other hominin species at BRT. The new material demonstrates that overall, *A. deyiremeda* was dentally and postcranially more primitive than *A. afarensis*, particularly in aspects of canine and premolar morphology, and in its retention of pedal grasping traits. Furthermore, the low and less variable distributions of its dental enamel $\delta^{13}C$ values are similar to those from *Ardipithecus ramidus* and *Australopithecus anamensis*, indicating a reliance on $C_3$ foods. This suggests that *A. deyiremeda* had a dietary strategy similar to the earlier *A. ramidus* and *A. anamensis*. The BRT foot and its assignment to *A. deyiremeda* provides conclusive evidence that arboreality was a significant component of the positional behaviour of this australopith, further corroborating that some degree of arboreality persisted among Pliocene hominins[1,3–7].

Hominin fossil discoveries in the past two decades suggest that multiple contemporaneous species existed in eastern Africa during the mid-Pliocene[1,2,8], but their validity, except for *A. afarensis* (a well-known Pliocene hominin species) has been questioned on various grounds including inadequate morphological distinction, small sample size or poor preservation[9–11]. There appears to be a consensus, however, that the BRT foot (BRT-VP-2/73) from Woranso-Mille[2], which was not assigned to a species at the time of its initial publication, is the strongest evidence for the presence of a non-*A. afarensis* species during the mid-Pliocene of eastern Africa[1,2,12–14]. Some researchers have argued that the presence of human-like feet in some members of early *Homo*, variability in the foot morphology of australopiths and a foot with an opposable hallux in some of the earliest hominins such as *A. ramidus* all suggest diversity in pedal adaptations for bipedal locomotion[15]. More recent studies have further suggested that the BRT foot demonstrated the presence of variability in foot morphology and bipedal locomotor adaptation among species of *Australopithecus*[9,16,17], whereas others have hinted that the BRT foot belonged to a late-surviving species of *Ardipithecus*[18] despite there being differences in the morphology of the first metatarsal and metatarsophalangeal joints[19].

One of the reasons why the BRT foot and several isolated teeth from the BRT localities were not assigned to *A. deyiremeda*, despite their provenience from the same horizon as one of the paratypes of the species, was the lack of diagnosable dentognathic specimens that could be directly compared with the holotype and paratype specimens of the species[2]. In the initial description of *A. deyiremeda*, it has been shown that some aspects of its maxillary and mandibular morphology were more derived than *A. afarensis*[1]. However, its second and third molars, including other teeth from BRT, overlapped, both in size and shape, with *A. afarensis* and other Pliocene hominins. Further fieldwork at Woranso-Mille, particularly at the BRT localities, has now resulted in the recovery of additional, and more diagnostic, dentognathic specimens from the same horizon as and immediately below the BRT foot (Fig. 1). On the basis of the provenience (vertical and horizontal), it is more than likely that the dentognathic specimens from the BRT localities and the BRT foot belong to the same species: *A. deyiremeda*. The BRT hominins retain more primitive (*A. anamensis*-like) dental features than *A. afarensis*, and there is now evidence that like *A. anamensis*, they also had a $C_3$-dominated dietary adaptation.

## Provenience and geological age

Most of the hominin specimens from BRT (BRT-VP-1 and BRT-VP-2) and Waytaleyta (WYT-VP-2) are surface finds that have weathered out of sandstone horizons along an approximately 30-m-thick section above a thin tuff, which has been radiometrically dated to 3.469 ± 0.008 million

[1]Institute of Human Origins and School of Human Evolution and Social Change, Tempe, AZ, USA. [2]Department of Anthropology, Washington University in St. Louis, St. Louis, MO, USA. [3]Department of Earth, Environmental and Planetary Sciences, Case Western Reserve University, Cleveland, OH, USA. [4]Berkeley Geochronology Center, Berkeley, CA, USA. [5]Departament de Mineralogia, Petrologia i Geologia Aplicada Facultat de Ciències de la Terra, Universitat de Barcelona, Barcelona, Spain. [6]Department of Biology, University of Tampa, Tampa, FL, USA. [7]Department of Earth and Environmental Sciences, University of Michigan, Ann Arbor, MI, USA. ✉e-mail: yhaileselassie@asu.edu

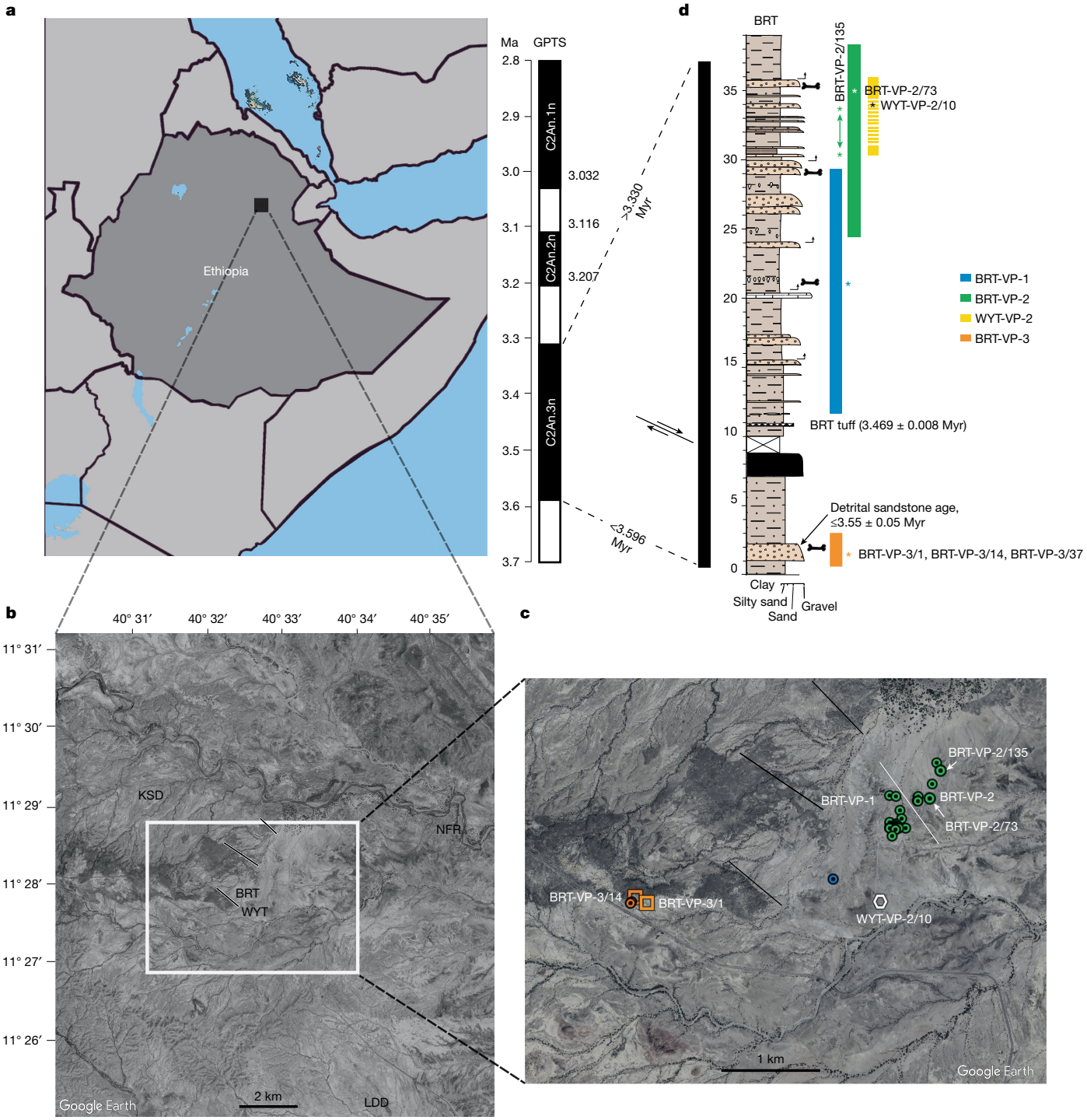


**Fig. 1 | Location map, stratigraphy and provenience. a**, Map of Ethiopia showing the location of the Woranso-Mille site. GPTS, geomagnetic polarity time scale. **b**, Satellite image showing the location of the BRT area (white rectangle) relative to other nearby mid-Pliocene localities. KSD, Korsi Dora (3.6 Myr); LDD, Leado Dido'a (3.4 Myr); NFR, Nefuraytu (3.3 Myr). The black lines indicate observed fault lines. *x*-axis, latitude; *y*-axis, longitude. **c**, A closeup view of the BRT area showing the distribution of fossil hominins on the landscape. The squares represent the holotype and paratype specimens of *A. deyiremeda*. The circles represent previously and newly discovered specimens including BRT-VP-2/73 and BRT-VP-2/135 shown by the white arrows. The white line is the boundary between BRT-VP-1 and BRT-VP-2, and the black lines are the faults shown in panel **b**. **d**, Composite stratigraphical section of the BRT and WYT localities. The coloured vertical bars show the vertical extent of each locality in the section. The maximum age of the hominins from these localities is 3.55 ± 0.05 Myr based on a new $^{40}Ar/^{39}Ar$ age from K-feldspar dating of grains in a detrital sandstone (see Supplementary Information, Supplementary Fig. 1 and Supplementary Data 1 for details). The entire stratigraphical sequence exhibits normal paleomagnetic polarity, suggesting that the hominins are 3.596–3.330 Myr (chron C2An.3n). Panels **b**,**c** were modified from Google Earth (Data SIO, NOAA. U/S/ Navy, NGA, GEBCO; Image IBCAO; Image Landsat/Copernicus).

years ago (Ma)[1,2] (Fig. 1, Supplementary Fig. 1 and Supplementary Data 1). Further detail is provided in Supplementary Information. Within this section, multiple fossiliferous sandstone horizons have been identified. The uppermost sandstone at BRT-VP-2, approximately 24 m above the dated tuff, yielded the BRT foot (BRT-VP-2/73). A lateral continuation of this sandstone is also exposed at the nearby WYT-VP-2 locality, where

**Table 1 | Newly recovered Pliocene hominins from BRT, Woranso-Mille, Ethiopia**

| Specimen number | Elements preserved | Discoverer | Year of discovery | Measurements (mm)[a] |
|---|---|---|---|---|
| BRT-VP-1/234 | Left lower M (mesial half) | Andarge Girmay | 2017 | NA |
| BRT-VP-1/256 | Left $M_3$ | Hamad Mee-ee | 2018 | MD=15.6 (15.8); BL=12.7 |
| BRT-VP-1/271 | Left mandibular fragment (edentulous) | Yohannes Haile-Selassie | 2018 | NA |
| BRT-VP-1/324 | Right $P_3$ | Sahleselassie Melaku | 2019 | MD=9.1; BL=10.3 (10.6) |
| BRT-VP-1/345 | Left mandible ($P_3$–$M_1$ root) | Ahmed Elema | 2023 | NA |
| BRT-VP-1/363 | Right mandibular fragment ($P_4$) | Andarge Girmay | 2024 | NA |
| BRT-VP-1/365 | Left $M^1$ | Kadir Helem | 2024 | MD=11.2; LaL=11.6 |
| BRT-VP-1/367 | Molar fragment | Kampiro Kayranto | 2024 | NA |
| BRT-VP-1/380 | Left $C^1$ | Ali Bereino | 2024 | MD=9.4; BL=9.3 (9.6) |
| BRT-VP-2/087 | Right ischium (juvenile) | Yohannes Haile-Selassie | 2011 | NA |
| BRT-VP-2/135[b] | Mandible with dentition (juvenile) | Diane Bernardoni | 2016 | $Ldc_1$: MD=5.3, LaL=5.1; $Rdm_2$: MD=9.55 (10.0), BL=8.7; $Ldm_2$: MD=10.2, BL=8.8; $LI_1$: MD=6.5, LaL=7.5; $RI_1$: MD=6.4, BL=7.7; $RC_1$: MD=8.6, BL=8.6; $LP_3$: MD=9.5 (9.0), BL=10.5 (9.6); $RP_3$: MD=9.3 (9.0), BL=10.7 (10.6); LP4: MD=9.3, BL=10.3; RP4: MD=8.8, BL=10.2; $LM_1$: MD=12.9, BL=11.9; $RM_1$: MD=12.4 (12.5), BL=12.0 |
| BRT-VP-2/150 | Frontal fragment | Yohannes Haile-Selassie | 2016 | NA |
| BRT-VP-2/200 | Occipital fragment | Kampiro Kayranto | 2018 | NA |

Upper and lower teeth are distinguished by superscript and subscript numbers, respectively. A superscript or subscript '1' associated with a canine (C/c) denotes upper and lower, respectively. [a]All measurements are in millimetres and those provided in parentheses are corrected for surface loss or crown expansion due to a crack (or cracks). [b]Dental dimensions of the canine and premolars (Ps) were taken from micro-CT images.
BL, buccolingual breadth; I, incisor; L, left; LaL, labiolingual breadth; M, molar; MD, mesiodistal length; NA, no data; R, right.

one of the paratype specimens of *A. deyiremeda* (WYT-VP-2/10) was found, less than 1 km southeast of the BRT foot. Other specimens from BRT-VP-2 and BRT-VP-1 (which samples the same section as BRT-VP-2 but goes slightly deeper) described in this and previous studies were recovered from a slope below the uppermost sandstone (green circles in Fig. 1c), suggesting that they probably eroded out from the upper sandstone. Only one hominin specimen at BRT-VP-1 was found at the lower level below two layers of sandstone horizons (blue circle in Fig. 1c) and it may have weathered out of any of the sandstones above it. The minimum age of the hominins from BRT-VP-1, BRT-VP-2 and WYT-VP-2 is 3.33 million years (Myr), as determined by paleomagnetic data[1,2] (Supplementary Information). Therefore, they are close in age to the nearby *A. afarensis*-bearing localities such as Leado Dido'a (LDD-VP-1; 3.42–3.330 Myr)[20] and Nefuraytu (NFR-VP-1; 3.330–3.207 Myr)[21], which are located 4.5–5 km to the south and east, respectively (Fig. 1b).

## Comparative description

A total of 25 hominin specimens, mostly isolated teeth, have been recovered from three BRT localities (BRT-VP-1, BRT-VP-2 and BRT-VP-3) thus far. Fourteen of these specimens, including the holotype and paratypes of *A. deyiremeda*, were reported in Haile-Selassie et al.[2]. Continued fieldwork since 2015 resulted in the discovery of additional, mostly dentognathic specimens (Table 1). A brief description of these specimens is provided in the Supplementary Information (also see Extended Data Figs. 1 and 2). One of the newly recovered specimens is a juvenile mandible, BRT-VP-2/135 (Fig. 2), which most likely eroded out from the same stratigraphic horizon as the BRT foot (BRT-VP-2/73; Fig. 1d). It was recovered approximately 300 m northeast of BRT-VP-2/73, and the difference in developmental age and distance between the two specimens shows that they did not belong to the same individual.

BRT-VP-2/135 consists of most of the corpus and a near-complete deciduous dentition, with the deciduous incisors ($di_{1-2}$) having already been exfoliated. The mandible also retains a total of 12 permanent teeth: the right and left incisors ($I_1$ and $I_2$; both erupting); the right canine still in the crypt and isolated mesial half of the left canine; the right and left third and fourth premolars ($P_3$ and $P_4$) still in the crypt; and the right and left first molars ($M_1$s). Both $M_1$s show slight wear facets on the protoconid and hypoconid, indicating that they were in occlusion with the maxillary teeth even though their root apices are still open. This mixed dentition allows an evaluation of the pattern of dental development as well as an estimate of the age of death of BRT-VP-2/135. When compared with other infant-to-juvenile hominin mandibular specimens at the same $M_1$ developmental state (the root three-quarters complete), the developmental status of BRT-VP-2/135 is similar to other early australopiths, specifically LH 3 (*A. afarensis*) and KNM-KP 34725 (*A. anamensis*), both of which evince a great ape-like pattern of relatively delayed incisor formation[22] (Extended Data Fig. 3 and Supplementary Table 1). An age at death estimate for BRT-VP-2/135 matches a chimpanzee-equivalent age of 4.47 years (range of 3.48–5.46 years), which is similar to age at death estimates for geologically younger hominins from South Africa including DNH 107 (4.82 years; *Paranthropus robustus*), Sts 24 (4.35 years; *Australopithecus africanus*) and StW 151 (4.65 years; early *Homo*) and to the geologically older KNM-KP 34725 (3.94 years; *A. anamensis*) from eastern Africa[23]. Details are provided in Supplementary Information.

The base of the BRT-VP-2/135 corpus and cortical bone in the symphyseal region are both missing. The lateral face of the corpus on the left side, however, is well preserved, showing the absence of the lateral corpus hollow (Fig. 2b), which is present in and diagnostic of both juvenile and adult mandibles of *A. afarensis*[24]. BRT-VP-2/258, a left edentulous mandible recovered during the 2025 field season, is about the same ontogenetic age and size of BRT-VP-2/135 and it also lacks the lateral corpus hollow (Extended Data Fig. 2l–m). BRT-VP-2/135, as does BRT-VP-2/258, lacks a deciduous canine ($d_c$)–deciduous first molar ($dm_1$) jugum (equivalent of $C_1$–$P_3$ jugum in adults) which is characteristic of *A. afarensis*[14,15]. *A. africanus* juvenile mandibles such as Taung also lack these features. A single mental foramen is positioned low on the corpus at the level of the distal $dm_2$, slightly posterior than in most *A. afarensis* juveniles where it is positioned at $dm_1$ or $dm_1$–$dm_2$. BRT-VP-2/258 is similar to the *A. afarensis* condition in this regard where the mental foramen is positioned mid-corpus at the mesial $dm_2$ level. The ascending ramus rises at the posterior $M_1$ level. The symphysis is damaged,

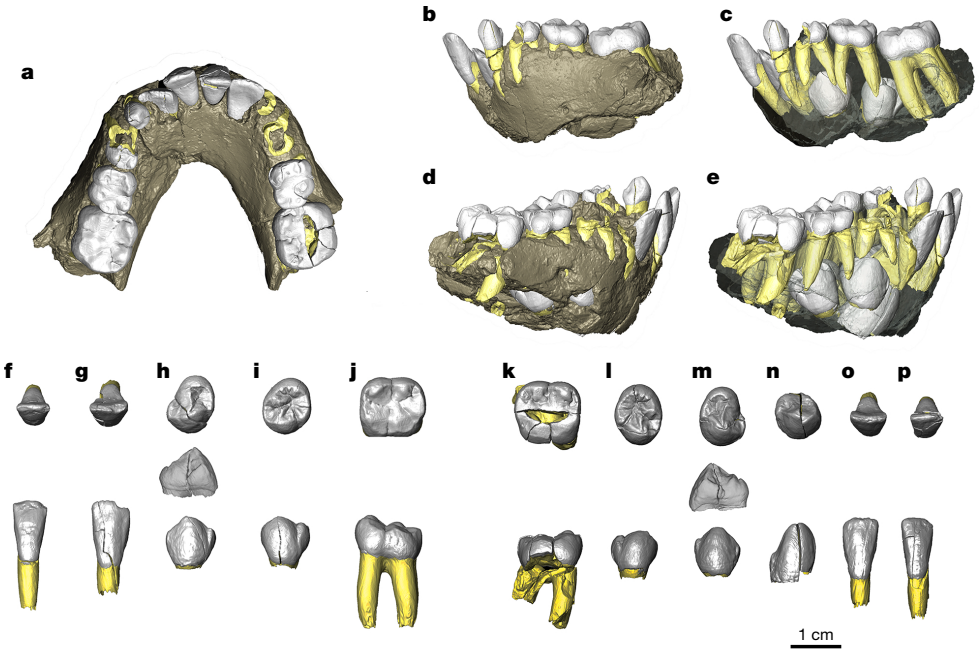


**Fig. 2 | The BRT-VP-2/135 mandible and its dentition. a**, Micro-CT scan rendering showing the occlusal view of the mandible. Tooth crowns are shown in white and preserved roots in yellow. **b**, Left lateral view of the mandible. **c**, Left lateral view of the mandible with crowns, roots and unerupted permanent dentition visible. **d**, Right lateral view of the mandible. **e**, Right lateral view of the mandible with crowns, roots and unerupted permanent dentition visible. Occlusal and labial or buccal views of permanent dentition are shown. **f**, Left $I_1$. **g**, Left $I_2$. **h**, Left $P_3$ (mesial view included). **i**, Left $P_4$. **j**, Left $M_1$. **k**, Right $M_1$. **l**, Right $P_4$. **m**, Right $P_3$ (mesial view included). **n**, Right canine. **o**, Right $I_2$. **p**, Right $I_1$.

although the preserved part shows that it is more posteriorly receding than in *A. afarensis* juveniles of comparable age.

### Deciduous teeth

The left $d_c$, distal half of the left $dm_1$ crown and both $dm_2$s of BRT-VP-2/135 are preserved. The occlusal crown outline of the $d_c$ is oval, comparable with the deciduous canines of *A. afarensis* and *A. anamensis*[25,26]. The heavily damaged $dm_1$ crown obscures any taxonomically informative morphology. The left $dm_2$ is preserved intact, whereas the enamel surfaces on the hypoconid, metaconid and mesial face of the right $dm_2$ are missing. The protoconid, hypoconid and hypoconulid of $dm_2$ all have variably sized dentine pits on their cusp tips. Morphologically, the occlusal outline of both $dm_2$s is broadly similar to those of *A. afarensis* and *A. anamensis* (there are no $dm_2$s reported for *A. ramidus*). The $dm_2$s of BRT-VP-2/135 are, however, mesiodistally shorter and much smaller in crown area, falling outside the known range of *A. afarensis*[27] and *A. africanus*[28], but within the known range of *A. anamensis*[29] (Fig. 3a and Supplementary Table 2).

### Incisors

The central incisors of BRT-VP-2/135 are emerging and close to the level of the occlusal plane, whereas the lateral incisors are only slightly beyond alveolar emergence. The incisor crowns are absolutely larger than those of *A. ramidus* ($n = 4$)[18,30] but fall within the known range of *A. anamensis*[26,29] and *A. afarensis*[10,27].

### Canines

The canines of BRT-VP-2/135, generated from high-resolution micro-computerized tomography (micro-CT) visualization, lack prominent lingual relief with only a thin, posteriorly positioned vertical ridge present, demarcating a distally placed vertical lingual groove (Extended Data Fig. 4). This is in stark contrast to the lower canines of *A. afarensis* that have prominent lingual relief with a centrally positioned thick vertical lingual ridge[25] creating prominent mesial and distal vertical lingual grooves (Extended Data Fig. 4d,e). The lack of lingual relief on the canines has been described as characteristic of both upper and lower canines of *A. deyiremeda*[1]. The lingual face and wear pattern of an isolated upper canine, BRT-VP-1/380, is also similar to *A. anamensis* canines such as KNM-KP 58309 and MRD-VP-1/1 in its lingual profile and wear pattern (Extended Data Fig. 5). Generally, the upper and lower canine crowns of *A. deyiremeda* are absolutely smaller than *A. ramidus* and other australopiths (see Fig. 4a–c for $C^1$ dimensions). Morphologically, however, the height of the mesial crown shoulders relative to the overall crown height on both upper and lower canines is within the range of variation seen in *A. afarensis*.

### Premolars

Both $P_3$s of BRT-VP-2/135, also generated from micro-CT visualization, and BRT-VP-1/324 have large anterior foveae and diminutive to absent metaconids. Furthermore, in both left and right $P_3$s of BRT-VP-2/135 and BRT-VP-1/324, the protoconid is positioned centrally and the transverse crest is oriented distolingually, whereas in *A. afarensis*, the protoconid apex is positioned more mesially in most $P_3$s even though some specimens such as A.L. 128-23 and A.L. 288-1i have centrally positioned protoconid apices (Extended Data Fig. 6). However, these specimens—like all other known *A. afarensis* $P_3$s—possess a transverse crest that forms less than 90° with the mesial protoconid crest (64.3–88.6° ($n = 12$) with an average of 76° and standard deviation of 7.6°), whereas in *A. ramidus*, *A. anamensis* and the $P_3$s of BRT-VP-2/135, it is more than 90° (Extended Data Fig. 6). In the $P_3$s from BRT, the mesial marginal ridge is also weak, and when viewed mesially, the anterior fovea is diamond shaped because of the steeply sloped buccal and weakly developed lingual segments of the mesial marginal ridge (Fig. 2h,m). All of these features are frequently seen in the $P_3$s of *A. anamensis* from Kanapoi as well as in *Pan troglodytes*[31]. The $P_3$ of the paratype mandible of *A. deyiremeda* (BRT-VP-3/14) also has a weakly developed metaconid, poorly definable lingual segment of the mesial marginal ridge whose mesial and distal segments are angled to the base of the crown, and distolingually oriented transverse ridge (Extended Data Fig. 6b). It is also high-crowned relative to its mesiodistal dimension, similar to

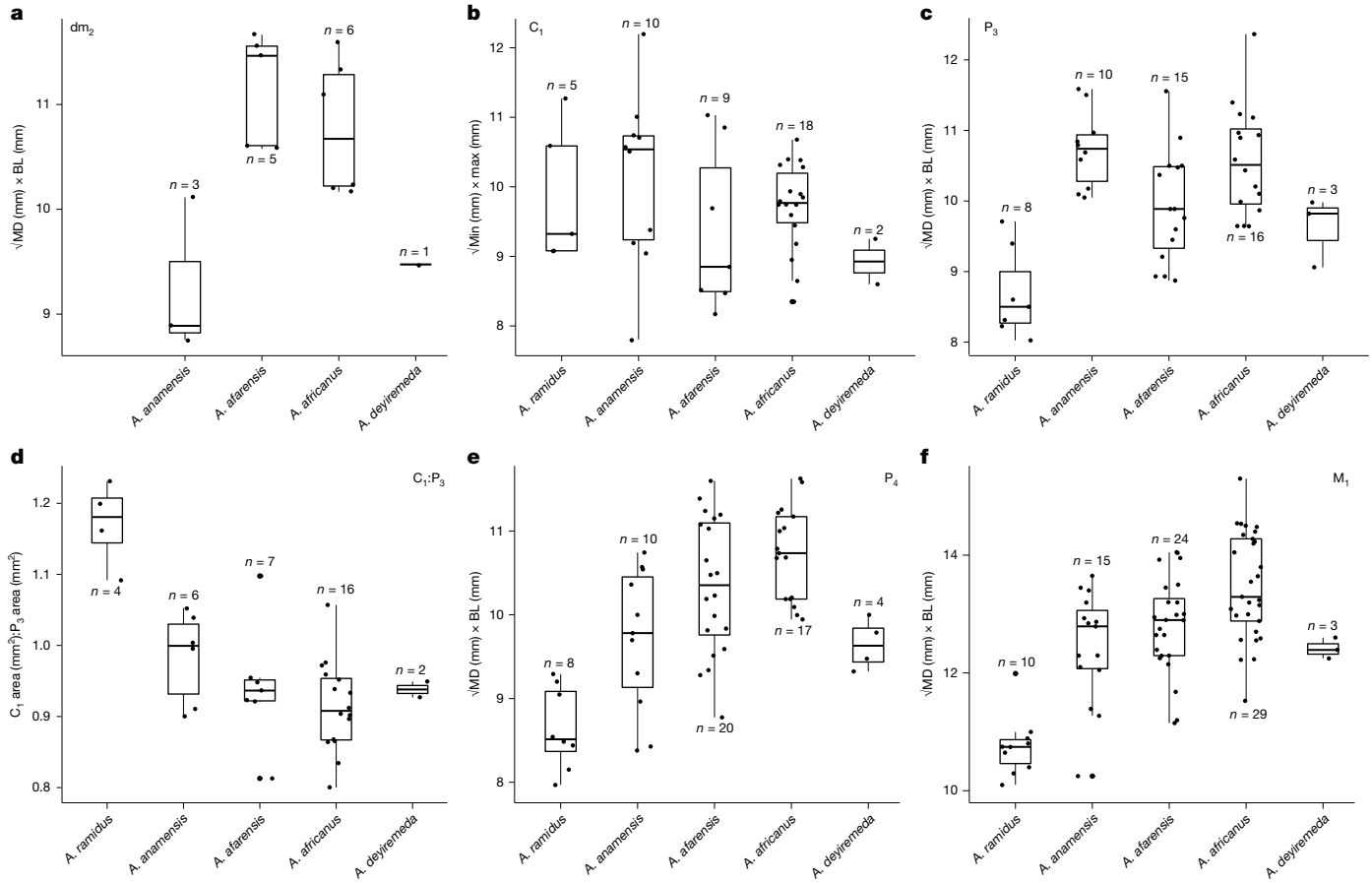


**Fig. 3 | Quantitative comparison of the lower dentition in early hominins.** **a**–**f**, Box-and-whisker plots of crown area of the $dm_2$ (**a**), $C_1$ (**b**), $P_3$ (**c**), $C_1$:$P_3$ ratio (**d**), $P_4$ (**e**) and $M_1$ (**f**) in *A. ramidus*, *A. anamensis*, *A. afarensis* and *A. africanus* compared with *A. deyiremeda*. The box in each plot represents the first to third quartiles of the dimensions, the line inside the box shows the median, and the horizontal lines outside the box represent the maximum and minimum values. The sample size is indicated by *n*. A statistical summary of the dental metrics used for this figure is provided in Supplementary Table 2 and Supplementary Data 2. The data were compiled from refs. 18,30 (*A. ramidus*), refs. 26,29 (*A. anamensis*), refs. 10,20,21,27 (*A. afarensis*) and ref. 28 (*A. africanus*).

the BRT-VP-2/135 $P_3$s. Although substantial intraspecific variation in the $P_3$ crown shape and occlusal morphology has been documented in *A. anamensis* and *A. afarensis*[27,29], as well as in *A. ramidus*[30], a few features distinguish the $P_3$s of these two species. For example, the $P_3$s of early *A. anamensis* from Kanapoi have relatively large anterior fovea and the metaconid is either absent or incipient when present[26]. Such intraspecific variation is also observed in the $P_3$s from BRT. Overall, however, the occlusal morphology and shape of the BRT $P_3$s are more similar to those of *A. ramidus* and *A. anamensis* than of *A. afarensis* (Extended Data Fig. 6). In terms of crown size, the $P_3$s from BRT are on the lower size range of australopiths but larger than those of *A. ramidus* (Fig. 3c). However, the latter species has larger canines relative to the size of the $P_3$ (Fig. 3d).

The $P_4$ crowns of BRT-VP-2/135 (also generated from micro-CT visualization) and other isolated $P_4$s (for example, BRT-VP-1/120; Extended Data Fig. 6b) have an oval occlusal crown outline, similar to *A. ramidus* and most *A. anamensis* $P_4$s (for example, KNM-KP 53160, KNM-KP 29286 and KNM-ER 20342). Another $P_4$, BRT-VP-1/363, is more likely the same individual as BRT-VP-1/2 based on its provenience and matches the latter in its preserved occlusal surface (Extended Data Figs. 1c and 2f). The preserved $P_4$ on one of the paratypes of *A. deyiremeda* (BRT-VP-3/14) also appears to have had an oval outline even though it is moderately damaged. By contrast, most *A. afarensis* $P_4$s have either a rhomboidal or square occlusal outline (Extended Data Fig. 6). In terms of their crown size, however, the BRT $P_4$s fall within the known range of *A. anamensis*, *A. afarensis* and *A. africanus* (Fig. 3e and Supplementary Data 2).

BRT-VP-2/89 (Extended Data Fig. 1j) is a complete $P^4$ crown germ that is morphologically indistinguishable from the previously reported $P^4$ (BRT-VP-3/37) of *A. deyiremeda*[1] and the $P^4$s of *A. anamensis* and *A. afarensis*. Its preserved crown dimensions are much larger than *A. ramidus*[30] but fall within the range of *A. anamensis*[26] and *A. afarensis*[10] (Extended Data Fig. 1j and Supplementary Data 2).

### Molars

Upper and lower molars of mid-Pliocene australopiths do not show significant metric and morphological variation. The size of two measurable $M_1$s from BRT fall within the known range of *Australopithecus* species but larger than those of *A. ramidus* (Fig. 3f). This was also the case with the molars associated with the paratype mandible of *A. deyiremeda*[1]. However, upper molars of the holotype of *A. deyiremeda* (BRT-VP-3/1) have been shown to be smaller than other australopiths[1]. BRT-VP-1/365 is one of the newly found $M^1$s and its size is only slightly larger than the $M^1$ of BRT-VP-3/1 (Fig. 4d–f and Supplementary Data 2). Both molars are also buccolingually narrower than all known australopiths (Fig. 4e). This is one of the diagnostic features of *A. deyiremeda*.

## Postcranial evidence

Two postcranial specimens have been recovered from BRT-VP-2. One of these is the partial foot (BRT-VP-2/73) previously described by Haile-Selassie et al.[2]. The second specimen (BRT-VP-2/87) is a right ischium of a juvenile individual found from the same locality and

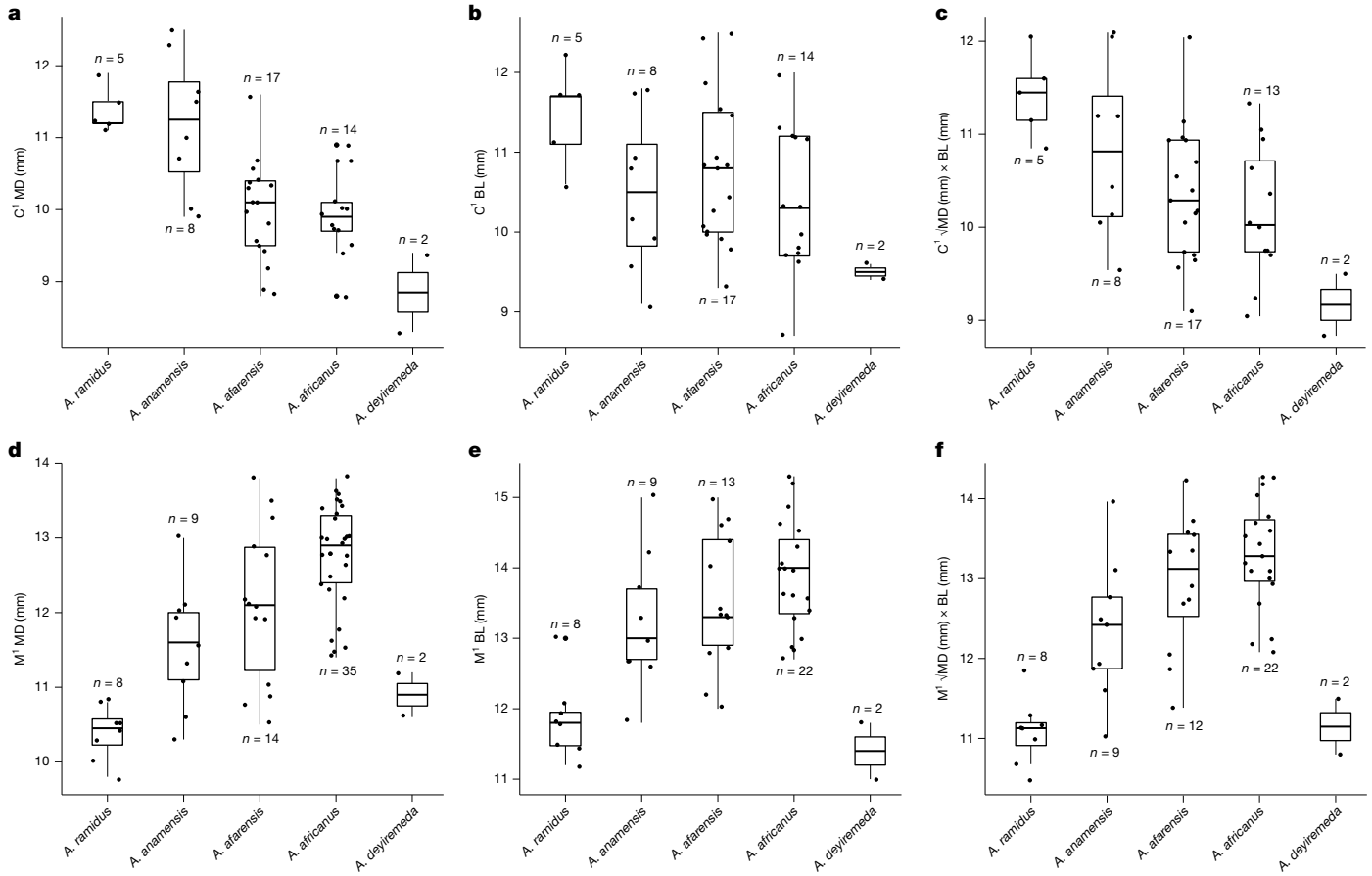


**Fig. 4 | Upper canine and M¹ size comparisons. a–f**, Box-and-whisker plots showing upper canine mesiodistal (MD) length (**a**), buccolingual (BL) breadth (**b**), the square root of MD multiplied by BL (**c**), M¹ MD length (**d**), BL breadth (**e**) and the square root of MD multiplied by BL (**f**) in *A. ramidus*, *A. anamensis*, *A. afarensis* and *A. deyiremeda*. Note that *A. deyiremeda* has the smallest upper canines and M¹s in the comparative sample. The box in each plot represents the first to third quartiles of the dimensions, the line inside the box shows the median, and the horizontal lines outside the box represent the maximum and minimum values. The sample size is indicated by *n*. A statistical summary of dental metrics used for this figure is provided in Supplementary Table 3, and the data were compiled from refs. 18,30 (*A. ramidus*), refs. 26,29 (*A. anamensis*), refs. 10,20,21,27 (*A. afarensis*) and ref. 28 (*A. africanus*).

horizon as the partial foot. A detailed description of BRT-VP-2/87 is provided in Supplementary Information (see also Extended Data Figs. 7 and 8). The partial foot displays morphological features that suggest a greater ability for grasping than modern humans and most fossil hominins[2,32]. These features include relatively long, sagittally curved pedal proximal phalanges; increased diaphyseal torsion and curvature in the transverse plane curvature of the second metatarsal (MT2); increased curvature in the sagittal plane of the MT1 diaphysis; increased mediolateral curvature of the MT1 proximal articular facet; and a gracile hallucal proximal phalanx with diaphyseal curvature also in the sagittal plane. This is in stark contrast to the foot morphology of *A. afarensis*[33] and provides further evidence for Pliocene hominin locomotor diversity (see Supplementary Information for further discussion).

The divergent hallux of *A. ramidus* (ARA-VP-6/500)[34] clearly differs from the comparatively more adducted, less mobile, hallux of *A. afarensis*, principally based on the morphology of the medial cuneiform (A.L. 333-28) and its articular relationship with the MT1 (A.L. 333-54). The MT1s assigned to *A. ramidus* from Aramis (ARA-VP-6/500-089)[34] and As Duma (GWM67/P2k)[35] display paired articular facets on the dorsal side of the bone divided by what Lovejoy et al.[34] refer to as a nonsubchondral isthmus (Extended Data Fig. 9). The expression of this MT1 head articular surface variation is hypothesized to reflect a divergent hallux as observed among extant African apes with arboreal foot-grasping adaptations[34]. Although there are subtle differences between the MT1 heads of the Aramis and As Duma specimens, including slightly increased dorsal doming in the latter, the BRT MT1 head is derived towards later hominins in lacking a nonsubchondral isthmus combined with mild dorsal doming and a more mediolaterally continuous MT1 head contour that bears resemblance to StW 595 (*A. africanus*) from Sterkfontein[8]. The MT2 of the BRT foot is also morphologically similar to StW 89 (refs. 2,32), another presumed *A. africanus* specimen from Sterkfontein. A multivariate analysis of 16 MT1 and fourth proximal phalanx (PP4) variables preserved across the partial feet of early hominins demonstrates that the *A. afarensis* (A.L. 333-115) and the BRT foot are both derived in the direction of modern humans relative to *A. ramidus* (ARA-VP-6/500). The placement of the BRT foot in the multivariate analysis is consistent with our observations of its more derived MT1 morphology than *A. ramidus* (Fig. 5).

The presence of metatarsal head dorsal doming—albeit minimal—and non-hallucal proximal phalanges with dorsally oriented proximal articular facets indicate an increased range of dorsiflexion at the metatarsophalangeal joint, which occurs during push-off among plantigrade bipeds[36] and digitigrade quadrupeds[33]. The combination of a relatively long MT4 and short MT1 implies that the oblique axis of the foot might have been used during the push-off period of the bipedal stance phase of the BRT hominin[2,37]. Although the torsion of MT4 of the BRT foot is consistent with the presence of a transverse arch that enhances midfoot stiffness during push-off[38], its diaphysis is relatively long and slender and it preserves features that do not align with a rigid midfoot, such as a dorsal portion of the proximal articular surface that is mediolaterally

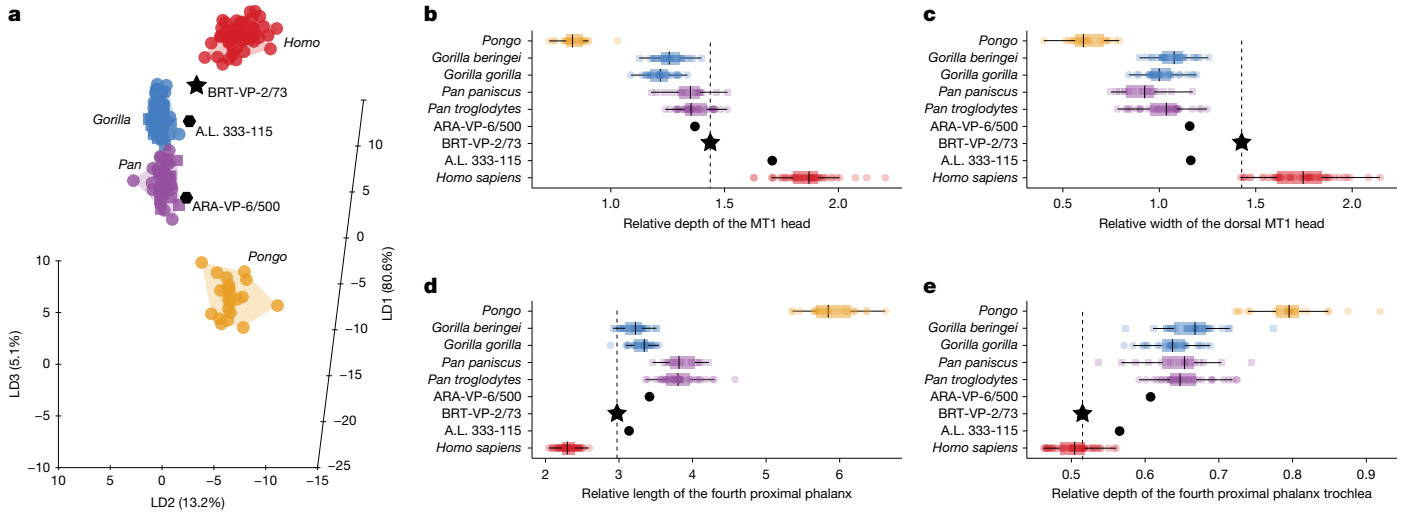


**Fig. 5 | Multivariate analysis of foot morphology in early hominins. a**, The first three dimensions of the linear discriminant (LD1–3) analysis represent 98.9% of the sample variance. **b**, BRT-VP-2/73 has a relatively shallow MT1 head similar to ARA-VP-6/500 and African apes, and unlike A.L. 333-115 and *Homo sapiens*. **c**, BRT-VP-2/73 has a relatively wide MT1 head, overlapping with *H. sapiens*, whereas A.L. 333-115 and ARA-VP-6/500 have narrower, more African ape-like MT1 heads. **d**, The relative length of the BRT-VP-2/73 PP4 is reduced compared with ARA-VP-6/500 and A.L. 333-115, falling at the low end of the *Gorilla* distributions. **e**, The relative depth of the PP4 trochlea is reduced in BRT-VP-2/73 compared with ARA-VP-6/500 and A.L. 333-115. All linear distances are scaled by the geometric mean. The box-and-whisker plots display the median, interquartile range and range, along with individual values. The star and dashed vertical line indicate the values for BRT-VP-2/73, whereas the black circles are the other fossil hominins in panels **b**–**e**.

curved, and a diaphysis that lacks a plantar orientation relative to its base. Likewise, the distal end displays a dorsomedial metatarsal head ridge that recalls the condition observed in some gorillas. Collectively, these lateral forefoot and midfoot traits suggest that the BRT hominin lacked the structural longitudinal arch and derived push-off morphology of the *A. afarensis* specimen A.L. 333-160 (ref. 39) and might have retained some midfoot mobility useful for climbing[32].

## Taxonomy and phylogenetic relationships

*A. afarensis* and *A. deyiremeda* have been identified from 3.5 to 3.3 Myr localities at Woranso-Mille[1,20,21]. The specimens assigned to *A. deyiremeda* derive from one of the localities at BRT (BRT-VP-3) and a slightly younger locality (WYT-VP-2), providing an age to the species between 3.5 and 3.3 Myr[1]. The specimens from BRT-VP-1 and BRT-VP-2 described here and in Haile-Selassie et al.[1,2] are from a horizon that is contemporaneous with WYT-VP-2 (3.47–3.33 Myr) where one of the paratype specimens of *A. deyiremeda* has been found. Furthermore, most of the newly recovered dental and mandibular remains retain morphological features that are diagnostic of *A. deyiremeda*. Among the dentognathic features shared with *A. deyiremeda* are premolars with more primitive occlusal morphology compared with the contemporaneous *A. afarensis*, canines with less lingual relief, small $M^1$s that are buccolingually narrow, mandibular body lacking lateral corpus hollow, and an anteriorly positioned ascending ramus root. The new dentognathic remains described here derive from the same stratigraphical unit as, and in close spatial proximity to, BRT-VP-2/73 (Fig. 1), suggesting that the latter can be confidently assigned to the same species. The absence of compelling evidence for the presence of more than one hominin species at the BRT localities also supports this assignment. The primitive aspects of the BRT foot could suggest a taxonomic attribution to a late-surviving species of *Ardipithecus*, but our understanding of the foot morphology of Pliocene hominins such as *A. ramidus* and *A. afarensis* is far from complete, and the pedal remains of *A. anamensis* are virtually unknown except for a fragmentary metatarsal shaft and an eroded distal phalanx from Asa Issie[40].

The inclusion of the BRT foot in *A. deyiremeda* further demonstrates that the latter species is also more primitive in its foot morphology than *A. afarensis*. Conversely, some aspects of the MT1 and MT2 of BRT-VP-2/73 are similar to *A. africanus* from Sterkfontein than to *A. afarensis*. *A. deyiremeda* and *A. africanus* have also previously been shown to be similar in maxillary shape than either is to *A. afarensis*[41,42]. A parsimony analysis to assess the phylogenetic position of *A. deyiremeda* has previously shown that it is a sister to a clade containing *A. africanus*, *Paranthropus* and *Homo*[1] with some dentognathic homoplasy. The inclusion of BRT-VP-2/73 in the *A. deyiremeda* hypodigm and its morphological similarity in some aspects of its morphology to *A. africanus* further highlights close relationship between these two taxa.

## Diet in *A. deyiremeda*

Habitat reconstruction of Pliocene hominins using different paleontological and geological proxies have shown that different hominins lived in a range of habitats. Although morphological approaches have traditionally been used for dietary reconstructions[43,44], carbon isotope data have been shown to provide a refined dietary signal[43–47], particularly powerful when the number of dental specimens is limited. Among Pliocene hominins, dietary adaptations of *A. deyiremeda* remain unknown even though two previously analysed isolated hominin teeth

**Table 2 | Stable carbon and oxygen isotopic data of fossil hominin teeth from BRT-VP-1 and BRT-VP-2**

| Specimen number | Element sampled | $\delta^{13}C_{VPDB}$ (‰) | $\delta^{18}O_{VPDB}$ (‰) |
|---|---|---|---|
| BRT-VP-1/1[a] | Left $M_3$ | −11.3 | −7.0 |
| BRT-VP-1/2 | Left $P_4$ | −9.3 | −3.1 |
| BRT-VP-1/18[a] | Left $M^2$ | −10.1 | −4.0 |
| BRT-VP-1/31 | Molar fragment | −12.4 | −3.6 |
| BRT-VP-1/118 | Left $M_3$ fragment | −8.8 | −3.6 |
| BRT-VP-1/234 | Left $M_1$ or $M_2$ mesial half | −9.8 | −4.4 |
| BRT-VP-1/256 | Left $M_3$ | −10.3 | −4.4 |
| BRT-VP-2/89 | Right $P^4$ | −9.5 | −4.6 |

[a]Data initially reported by Levin et al.[47].

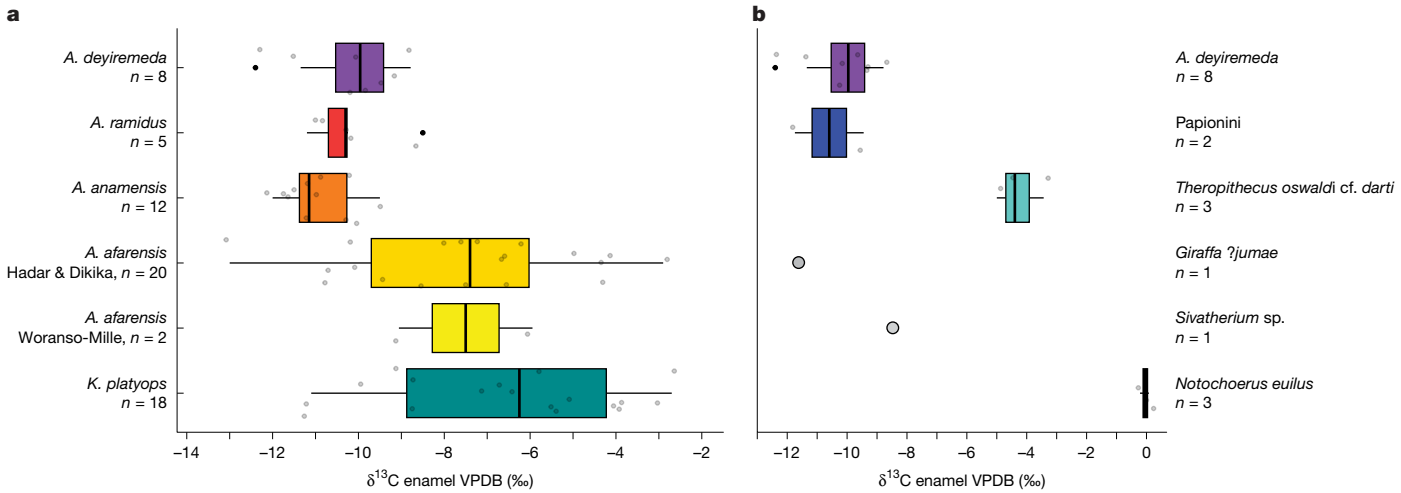


**Fig. 6 | Boxplot of $\delta^{13}C$ values for tooth enamel. a**, $\delta^{13}C$ values of new *A. deyiremeda* teeth from BRT-VP-1 and BRT-VP-2 plotted with published data from other early and middle Pliocene hominins from eastern Africa. **b**, Other mammal teeth analysed from BRT-VP-1 and BRT-VP-2. For panel **a**, $\delta^{13}C$ data came from the following sites and studies: for *A. ramidus*, Aramis, Sagantole Fm[48]; for *A. anamensis*, Turkana (Koobi Fora Formation and Kanapoi Fms)[44]; for *A. afarensis*, Hadar Fm at Hadar and Dikika[46] and from two sites at Woranso-Mille (LDD and NFR)[47]; and for *K. platyops*, Nachukui Fm[44]. The hominin data from other study areas are plotted using the compilation by Levin et al.[47]. The previously published data from other mammal teeth analysed from BRT-VP-1 and BRT-VP-2 also came from ref. 47. The boxplots represent median values with the middle line, and the interquartile ranges as the horizontal edges of the box, and the minimum and maximum values are plotted as lines extending from the boxes, with outliers plotted outside these lines. Jitter points are plotted to visualize the distribution of all data points and the number of analyses. Only single points are plotted for cases where $n = 1$. VPDB, Vienna Pee Dee Belemnite international reference standard.

from BRT-VP-1 yielded $\delta^{13}C$ values < −10‰, indicative of a reliance on $C_3$ foods[47]. For this study, an additional six *A. deyiremeda* teeth from the two BRT localities (BRT-VP-1 and BRT-VP-2) were sampled for their isotopic composition. Combined with previously published data from isolated hominin teeth from BRT-VP-1 ($n = 2$), presumably belonging to *A. deyiremeda*[47], the mean $\delta^{13}C$ value for the BRT teeth is −10.2 ± 1.2‰ and range from −12.4 to −8.8‰ ($n = 8$; Table 2 and Fig. 6a). Compared with other mammal teeth sampled for isotopic study from these localities ($n = 10$), the hominins yield some of the lowest $\delta^{13}C$ values and indicate a diet dominated by $C_3$ resources, despite the presence of other mammals that depended on either a mix of $C_3$–$C_4$ resources (for example, *Theropithecus oswaldi* cf. *darti*) or pure $C_4$ graze (*Notochoerus euilus*; Fig. 6b).

Compared with other early and mid-Pliocene hominins at Woranso-Mille and elsewhere in the Afar, and from eastern Africa more broadly, the $\delta^{13}C$ values from the BRT hominin teeth are indistinct from distributions of $\delta^{13}C$ values from *A. ramidus* and *A. anamensis* teeth, but distinct from $\delta^{13}C$ values for *A. afarensis* and *Kenyanthropus platyops* (Table 3 and Fig. 6a). *A. anamensis* ($n = 12$)[44–46] and earlier hominins such as *A. ramidus* ($n = 5$)[48] relied mainly on $C_3$ food resources even though *A. anamensis* may also have consumed a substantial amount of $C_4$ resources[49]. Species such as *A. afarensis* and *Kenyanthropus platyops* utilized a wide range of both $C_3$ and $C_4$ resources[44,46]. The lower $\delta^{13}C$ values of the BRT hominin teeth, with more limited distributions, and their similarity to those from *A. ramidus* and *A. anamensis*, indicate that the BRT hominins may have retained dietary strategies of these older (more primitive) hominins, corroborating morphological observations.

## Discussion and conclusion

Newly discovered 3.47–3.33 Myr fossil hominin specimens from mid-Pliocene Woranso-Mille have been described. Comparative analysis of these mostly dentognathic remains shows that they can confidently be assigned to *A. deyiremeda*, based on features diagnostic of the species (for example, lack of lingual relief on both upper and lower canines and relatively smaller teeth). Although *A. deyiremeda* appears to be more derived than *A. afarensis* in certain maxillary (low, anterior zygomatic origin)[1,41,42] and mandibular traits (lack of lateral corpus hollow)[1], this study found that its premolar occlusal morphology (oval $P_4$ outline and reduced or absent $P_3$ metaconid) resembles the earlier *A. anamensis* and *A. ramidus*, indicating that it is dentally more primitive than *A. afarensis*.

Enamel isotope analysis also suggests that *A. deyiremeda* had a $C_3$-dominated diet, similar to *A. anamensis* and *A. ramidus*. The BRT partial foot (BRT-VP-2/73) is assigned to *A. deyiremeda* due to its temporal and spatial association with dentognathic materials assigned to the species. This assignment provides the most compelling evidence for multiple bipedal adaptations in *Australopithecus*, despite shared postcanine megadontia. Although the exact timing of dental enlargement in australopiths remains uncertain, it probably reflects adaptation to changing environments and diverse dietary niches. Previous studies have highlighted variability in early australopith foot morphology, indicating diverse bipedal forms, each with variable pelvic, limb and foot morphology[50]. Current evidence has suggested that some species—such as *A. deyiremeda*, *A. africanus* and *Australopithecus sediba*—remained capable climbers, whereas others such as *A. afarensis* were more terrestrial. The mosaic craniodental and postcranial morphology of *A. deyiremeda* raises questions about skeletal integration, and confirms that postcanine megadontia and obligate, human-like bipedality did not evolve simultaneously. The origin of *Australopithecus* correlates with

**Table 3 | Summary statistics for $\delta^{13}C$ values of hominin teeth compared in this study**

| Taxon | *n* | Mean | Median | s.d. | Minimum | Maximum |
|---|---|---|---|---|---|---|
| *A. deyiremeda* | 8 | −10.2 | −10.0 | 1.2 | −12.4 | −8.8 |
| *A. ramidus* | 5 | −10.2 | −10.3 | 1.0 | −11.2 | −8.5 |
| *A. anamensis* | 12 | −10.9 | −11.2 | 0.8 | −12.0 | −9.5 |
| *A. afarensis* (Hadar and Dikika) | 20 | −7.5 | −7.4 | 2.6 | −13.0 | −2.9 |
| *A. afarensis* (Woranso-Mille) | 2 | −7.5 | −7.5 | 2.2 | −9.1 | −5.9 |
| *K. platyops* | 18 | −6.6 | −6.3 | 2.7 | −11.1 | −2.7 |

increased craniodental size—possibly linked to selection for smaller canines and premolar molarization—preceding full obligate bipedality.

Although mid-Pliocene hominin paleobiology and locomotion remain incompletely understood[40], the BRT foot confirms the presence of multiple bipedal forms during the Pliocene. Further postcranial fossil discoveries, particularly of early species such as *A. anamensis*, will be crucial to fully understanding the origins of obligate human-like bipedality.

## Online content

Any methods, additional references, Nature Portfolio reporting summaries, source data, extended data, supplementary information, acknowledgements, peer review information; details of author contributions and competing interests; and statements of data and code availability are available at https://doi.org/10.1038/s41586-025-09714-4.


1. Haile-Selassie, Y. et al. New species from Ethiopia further expands middle Pliocene hominin diversity. *Nature* **521**, 483–488 (2015).
2. Haile-Selassie, Y. et al. A new hominin foot from Ethiopia shows multiple Pliocene bipedal adaptations. *Nature* **483**, 565–569 (2012).
3. Stern, J. T. Jr & Susman, R. L. The locomotor anatomy of *Australopithecus afarensis*. *Am. J. Phys. Anthropol.* **60**, 279–317 (1983).
4. Clarke, R. J. & Tobias, P. V. Sterkfontein member 2 foot bones of the oldest South African hominid. *Science* **269**, 521–524 (1995).
5. Zipfel, B. et al. The foot and ankle of *Australopithecus sediba*. *Science* **333**, 1417–1420 (2011).
6. DeSilva, J. M., Proctor, D. J. & Zipfel, B. A complete second metatarsal (StW 89) from Sterkfontein member 4, South Africa. *J. Hum. Evol.* **63**, 487–496 (2012).
7. McNutt, E. J. et al. Footprint evidence of early hominin locomotor diversity at Laetoli, Tanzania. *Nature* **600**, 468–471 (2021).
8. Leakey, M. G. et al. New hominin genus from eastern Africa shows diverse middle Pliocene lineages. *Nature* **410**, 433–440 (2001).
9. White, T. Early hominids — diversity or distortion? *Science* **299**, 1994–1997 (2003).
10. Kimbel, W. H., Rak, Y. & Johanson, D. C. *The Skull of* Australopithecus afarensis (Oxford Univ. Press, 2004).
11. Kimbel, W. H. et al. Was *Australopithecus anamensis* ancestral to *A. afarensis*? A case of anagenesis in the hominin fossil record. *J. Hum. Evol.* **51**, 134–152 (2006).
12. McNutt, E. J., Zipfel, B. & DeSilva, J. M. The evolution of the human foot. *Evol. Anthropol.* **27**, 197–217 (2018).
13. Wood, B. & Boyle, E. K. Hominin taxic diversity: fact or fantasy? *Am. J. Phys. Anthropol.* **159**, 37–78 (2016).
14. Alemseged, Z. Reappraising the palaeobiology of *Australopithecus*. *Nature* **617**, 45–54 (2023).
15. Harcourt-Smith, W. E. & Aiello, L. C. Fossils, feet and the evolution of human bipedal locomotion. *J. Anat.* **204**, 403–416 (2004).
16. DeSilva, J. M. et al. *Australopithecus sediba* — the anatomy of the lower limb skeleton of *Australopithecus sediba*. *Paleoanthropology* **2018**, 357–405 (2018).
17. DeSilva, J. M., McNutt, E. J. & Zipfel, B. in *The Evolution of the Primate Foot: Anatomy, Function, and Palaeontological Evidence* (eds Zeininger, A. et al.) 361–385 (Springer, 2022).
18. White, T. D., Lovejoy, C. O., Asfaw, B., Carlson, J. P. & Suwa, G. Neither chimpanzee nor human, *Ardipithecus* reveals the surprising ancestry of both. *Proc. Natl Acad. Sci. USA* **112**, 4877–4884 (2015).
19. Prang, T. C., Ramirez, K., Grabowski, M. & Williams, S. A. *Ardipithecus* hand provides evidence that humans and chimpanzees evolved from an ancestor with suspensory adaptations. *Sci. Adv.* **7**, eabf2474 (2021).
20. Melillo, S. M. et al. New Pliocene hominins from the Leado Dido'a area of Woranso-Mille, Ethiopia. *J. Hum. Evol.* **153**, 102956 (2021).
21. Haile-Selassie, Y. et al. Dentognathic remains of *Australopithecus afarensis* from Nefuraytu (Woranso-Mille, Ethiopia): comparative description, geology, and paleoecological context. *J. Hum. Evol.* **100**, 35–53 (2016).
22. Dean, M. C., Lim, S. Y. & Liversidge, H. M. Patterns of permanent incisor, canine and molar development in modern humans, great apes and early fossil hominins. *Arch. Oral Biol.* **143**, 105549 (2022).
23. Smith, T. M. et al. Dental ontogeny in Pliocene and early Pleistocene hominins. *PLoS ONE* **10**, e0118118 (2015).
24. Glowacka, H., Kimbel, W. H. & Johanson, D. C. in *Human Paleontology and Prehistory: Vertebrate Paleobiology and Paleoanthropology* (eds Marom, A. & Hovers, E.) 127–144 (Springer, 2017).
25. Johanson, D. C., White, T. D. & Coppens, Y. Dental remains from the Hadar Formation, Ethiopia: 1974–1977 collections. *Am. J. Phys. Anthropol.* **57**, 545–603 (1982).
26. Ward, C. V., Leakey, M. G. & Walker, A. Morphology of *Australopithecus anamensis* from Kanapoi and Allia Bay, Kenya. *J. Hum. Evol.* **41**, 255–368 (2001).
27. White, T. D. New fossil hominids from Laetoli, Tanzania. *Am. J. Phys. Anthropol.* **46**, 197–230 (1977).
28. Moggi-Cecchi, J., Grine, F. E. & Tobias, P. V. Early hominid dental remains from member 4 and 5 of the Sterkfontein Formation (1966–1996 excavations): catalogue, individual associations, morphological descriptions and initial metrical analysis. *J. Hum. Evol.* **50**, 239–328 (2006).
29. Ward, C. V., Manthi, F. K. & Plavcan, J. M. New fossils of *Australopithecus anamensis* from Kanapoi, West Turkan, Kenya (2003–2008). *J. Hum. Evol.* **65**, 501–524 (2013).
30. Suwa, G. et al. Paleobiological implications of the *Ardipithecus ramidus* dentition. *Science* **326**, 69–99 (2009).
31. Delezene, L. K. & Kimbel, W. H. Evolution of the mandibular third premolar crown in early *Australopithecus*. *J. Hum. Evol.* **60**, 711–730 (2011).
32. DeSilva, J., McNutt, E., Benoit, J. & Zipfel, B. One small step: a review of Plio-Pleistocene hominin foot evolution. *Am. J. Phys. Anthropol.* **168**, 63–140 (2019).
33. Latimer, B. & Lovejoy, C. O. Metatarsophalangeal joints of *Australopithecus afarensis*. *Am. J. Phys. Anthropol.* **83**, 13–23 (1990).
34. Lovejoy, C. O., Latimer, B., Suwa, G., Asfaw, B. & White, T. D. Combining prehension and propulsion: the foot of *Ardipithecus ramidus*. *Science* **326**, 72–72.e8 (2009).
35. Simpson, S. W., Levin, N. E., Quade, J., Rogers, M. J. & Semaw, S. *Ardipithecus ramidus* postcrania from the Gona Project area, Afar regional state, Ethiopia. *J. Hum. Evol.* **129**, 1–45 (2019).
36. Fernández, P. J. et al. Evolution and function of the hominin forefoot. *Proc. Natl Acad. Sci. USA* **115**, 8746–8751 (2018).
37. Latimer, B. & Lovejoy, C. O. Hallucal tarsometatarsal joint in *Australopithecus afarensis*. *Am. J. Phys. Anthropol.* **82**, 125–133 (1990).
38. Venkadesan, M. et al. Stiffness of the human foot and evolution of the transverse arch. *Nature* **579**, 97–100 (2020).
39. Ward, C. V., Kimbel, W. H. & Johanson, D. C. Complete fourth metatarsal and arches in the foot of *Australopithecus afarensis*. *Science* **331**, 750–753 (2011).
40. White, T. D. et al. Asa Issie, Aramis and the origin of *Australopithecus*. *Nature* **440**, 883–889 (2006).
41. Hanegraef, H., Leakey, M. G., Leakey, L. N. & Spoor, F. Mid-Pliocene hominin diversity revisited. *C. R. Paleovol.* **23**, 453–464 (2024).
42. Spoor, F., Leakey, M. G. & O'Higgins, P. Middle Pliocene hominin diversity: *Australopithecus deyiremeda* and *Kenyanthropus platyops*. *Phil. Trans. R. Soc. B* **371**, 20150231 (2016).
43. Bobe, R., Manthi, F. K., Ward, C. V., Plavcan, J. M. & Carvalho, S. The ecology of *Australopithecus anamensis* in the early Pliocene of Kanapoi, Kenya. *J. Hum. Evol.* **140**, 102717 (2020).
44. Cerling, T. E. et al. Stable isotope-based diet reconstructions of Turkana Basin hominins. *Proc. Natl Acad. Sci. USA* **110**, 10501–10506 (2013).
45. Sponheimer, M. et al. Isotopic evidence of early hominin diets. *Proc. Natl Acad. Sci. USA* **110**, 10513–10518 (2013).
46. Wynn, J. G. et al. Diet of *Australopithecus afarensis* from the Pliocene Hadar Formation, Ethiopia. *Proc. Natl Acad. Sci. USA* **110**, 10495–10500 (2013).
47. Levin, N. E., Haile-Selassie, Y., Frost, S. R. & Saylor, B. Z. Dietary change among hominins and cercopithecids in Ethiopia during the early Pliocene. *Proc. Natl Acad. Sci. USA* **112**, 12304–12309 (2015).
48. White, T. D. et al. Macrovertebrate paleontology and the Pliocene habitat of *Ardipithecus ramidus*. *Science* **326**, 67–93 (2009).
49. Quinn, R. L. Isotopic equifinality and rethinking the diet of *Australopithecus anamensis*. *Am. J. Phys. Anthropol.* **169**, 403–421 (2019).
50. Prang, T. C. The subtalar joint complex of *Australopithecus sediba*. *J. Hum. Evol.* **90**, 105–119 (2016).

# Methods

### Micro-CT scanning and visualization protocols

The BRT mandible (BRT-VP-2/135) was scanned (with permit from the Ethiopian Heritage Authority to Y.H.-S.) using a GE v|tome|x L300 industrial multiscale micro-CT scanner at the Pennsylvania State University Center for Quantitative Imaging with the following scan parameters: 150 kV, 200 μA, 0.2-mm Al filter, 2,400 projections, 5 frames averages per projection, detector timing of 500 ms and reconstructed with an isotropic voxel size of 32.5 μm. The data were segmented and a three-dimensional isosurface of the unerupted teeth and external surface of the mandible were created in Avizo v9.5 (Thermo Fisher Scientific). Enamel and dentine surfaces of erupted teeth were segmented using automated thresholding, whereas dental tissue boundaries for the unerupted dentition were segmented manually. All dental tissue boundaries (enamel, dentine and pulp) were manually traced approximately every ten slices and filled in using the interpolation tool. These interpolated regions were then visually inspected for boundary integrity and continuity and manually edited if needed. Cross-sectional images of each tooth were generated in Avizo v9.5 (Thermo Fisher Scientific) using the slice tool so that each cross-section captured the maximum extent of the dentine horn as close to the cusp tip as possible. Surface models of each tooth were exported and processed (spikes and small holes removed) in GeoMagic Wrap 2017.

### Enamel isotope sampling

Enamel from isolated fossil teeth sampled with a hand-held dental drill and diamond-burred bits, targeting broken surfaces where possible. Sample powders were treated with 3% hydrogen peroxide for 15 min and then with 0.1 M buffered acetic acid, rinsing three times after each treatment, and then dried at 60 °C overnight before analysis. Treated powders were then analysed on Kiel IV (15 min reaction in $H_3PO_4$ at 75 °C), coupled to a Thermo Fisher MAT 253 mass spectrometer at the University of Michigan Stable Isotope Laboratory and calibrated using calcite standards. Oxygen isotope values were calculated assuming a temperature-dependent acid fractionation factor for fossil teeth[51]. External precision of working enamel standards during the analysis were less than 0.4‰ and less than 0.15‰ for $\delta^{13}C$ and $\delta^{18}O$ values, respectively. Isotopic data are reported relative to the Vienna Pee Dee Belemnite standard.

Statistics were calculated in R (2024.04.2 + 764). The ± symbol indicates standard deviation. Statistics of difference were calculated using the unpaired Wilcoxon–Mann–Whitney rank-sum test, with significant distinctions set with $P = 0.05$.

### Multivariate analysis of partial feet

Linear discriminant analysis was used to test whether extant taxa (*H. sapiens* $n = 52$, *P. troglodytes* $n = 39$, *Pan paniscus* $n = 18$, *Gorilla gorilla* $n = 30$, *Gorilla beringei* $n = 31$ and *Pongo* spp. $n = 22$) could be separated using 16 MT1 and PP4 variables preserved among BRT-VP-2/73, A.L. 333-115 and ARA-VP-6/500. The variables include 5 MT1 variables (midshaft mediolateral width, midshaft dorsoplantar depth, dorsal head width, plantar head width and head dorsoplantar depth) and 11 PP4 variables (length, maximum dorsoplantar depth of base, dorsoplantar depth of proximal articular facet, maximum mediolateral width of base, mediolateral width of the proximal articular facet, midshaft mediolateral width, midshaft dorsoplantar depth, mediolateral width of trochlea, dorsoplantar depth of trochlea, diaphyseal curvature and a dorsal canting ratio). Diaphyseal curvature was calculated using measurement photographs, and the dorsal canting ratio is the ratio of the dorsal interarticular length to the plantar interarticular length. All linear measurements were scaled by a geometric mean composed of 14 measurements per individual. The pooled covariance matrix of the 16 variables was analysed using linear discriminant analysis in R v4.4.0.

### Reporting summary

Further information on research design is available in the Nature Portfolio Reporting Summary linked to this article.

## Data availability

All data used in this article are presented in the Supplementary Information. Request to access the three-dimensional scans of specimens included in this article should be sent to the Ethiopian Heritage Authority at yonasyilma2627@gmail.com.


51. Passey, B. H., Cerling, T. E. & Levin, N. E. Temperature dependence of oxygen isotope acid fractionation for modern and fossil tooth enamels. *Rapid Commun. Mass Spectrom.* **21**, 2853–2859 (2007).
52. Haile-Selassie, Y. et al. A 3.8-million-year-old hominin cranium from Woranso-Mille, Ethiopia. *Nature* **573**, 214–219 (2019).



**Acknowledgements** We thank the Ethiopian Heritage Authority of the Ethiopian Ministry of Tourism for permission to conduct field and laboratory work; the Afar people of Woranso-Mille and the Mille District administration for their hospitality; M. Mengesha for assisting in the geological work at BRT; the project's fieldwork crew members for their tireless support of field activities; T. White, G. Suwa and B. Asfaw for access to the original *A. ramidus* material and for providing images; C. Campisano for access to unpublished *A. afarensis* material; S. Melillo, C. Taylor, A. Slotter and D. Bernardoni for fossil recovery; S. Melaku of the Ethiopian Heritage Authority for access to the fossil collections housed in the Paleoanthropology Laboratory in Addis Ababa and facilitating isotope sampling; and T. Ryan and T. Stecko from the Penn State Center for Quantitative Imaging for assistance with computed tomography scanning. N.E.L. thanks K. Lohmann at the University of Michigan for assistance with isotope analysis. This research was supported by previous grants from the US National Science Foundation (BCS-1124705, BCS-1124713, BCS-1124716, BCS-1125157 and BCS-1125345) and The W. M. Keck Foundation.


**Author contributions** Y.H.-S., B.Z.S., A.D., L.G. and N.E.L. conducted the fieldwork and collected primary data. Y.H.-S., G.T.S. and T.C.P. did the comparative description of the hominins. A.R. performed the three-dimensional segmentation. N.E.L. carried out the isotopic analysis. A.D., L.G., B.Z.S. and N.E.L. worked on the stratigraphy, geochronology and magnetostratigraphy. All co-authors contributed to the writing of the manuscript.

**Competing interests** The authors declare no competing interests.


**Additional information**
**Supplementary information** The online version contains supplementary material available at https://doi.org/10.1038/s41586-025-09714-4.


**Correspondence and requests for materials** should be addressed to Yohannes Haile-Selassie.


**Peer review information** *Nature* thanks Thure Cerling and the other, anonymous, reviewer(s) for their contribution to the peer review of this work. Peer reviewer reports are available.

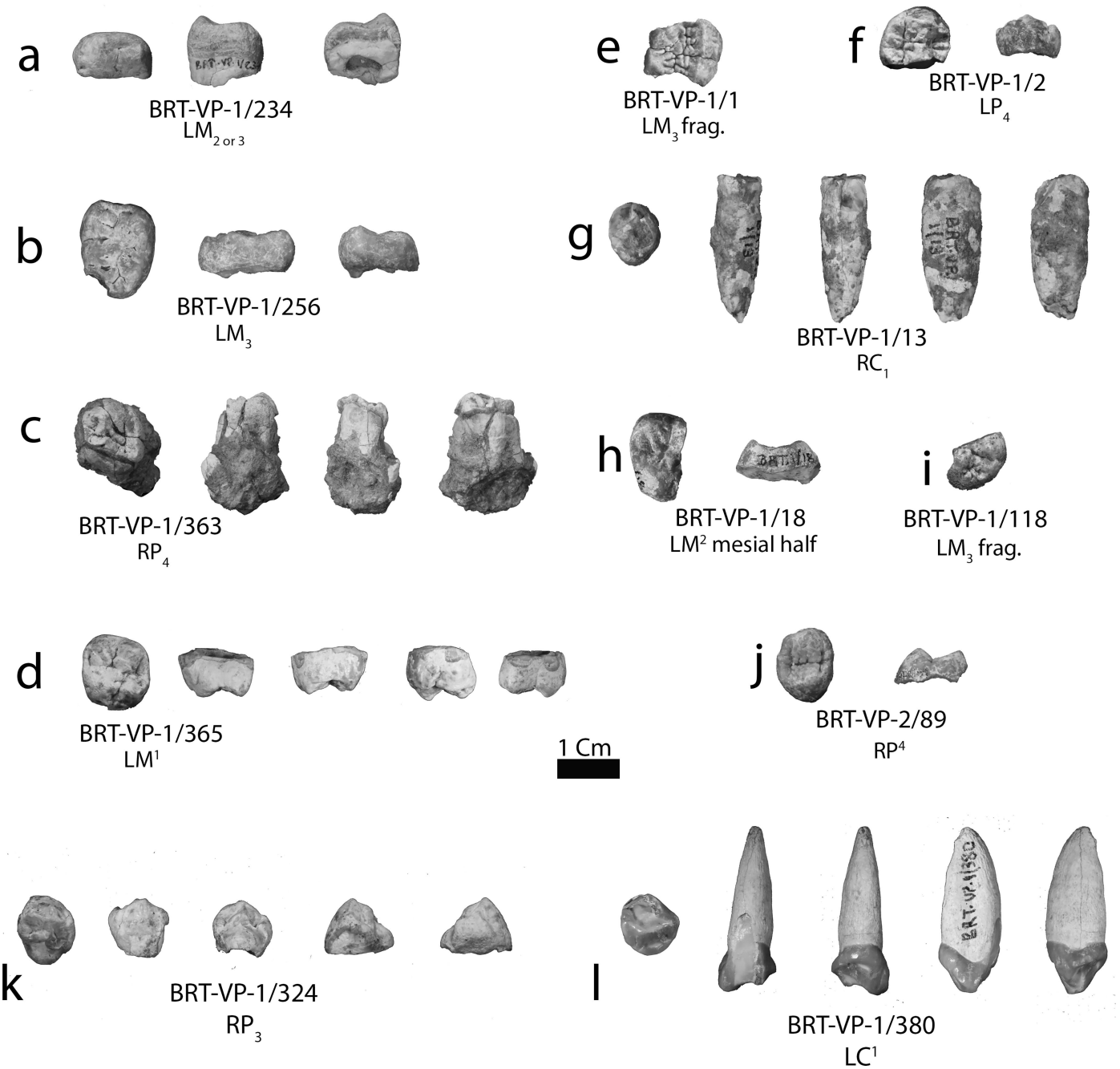


**Extended Data Fig. 1 | Dental specimens from BRT-VP-1 and BRT-VP-2.** **a**, BRT-VP-1/234 in occlusal, mesial, and distal views. **b**, BRT-VP-1/256 in occlusal, lingual and mesial views. **c**, BRT-VP-1/363 in occlusal, distal, lingual, and mesial views. **d**, BRT-VP-1/365 in occlusal, mesial, distal, lingual, and buccal views. **e**, BRT-VP-1/1 in occlusal view. **f**, BRT-VP-1/2 in occlusal and buccal views. **g**, BRT-VP-1/13 in occlusal, lingual, buccal, mesial, and distal views. **h**, BRT-VP-1/18 in occlusal and mesial views. **i**, BRT-VP-1/118 in occlusal view. **j**, BRT-VP-2/89 in occlusal and mesial views. **k**, BRT-VP-1/324 in occlusal, buccal, lingual, mesial, and distal views. **l**, BRT-VP-1/380 in occlusal, buccal, lingual, mesial, and distal views. Specimens **e-j** were listed in Table 1 in Haile-Selassie et al.[1]. Their brief description is provided in Supplementary Information.

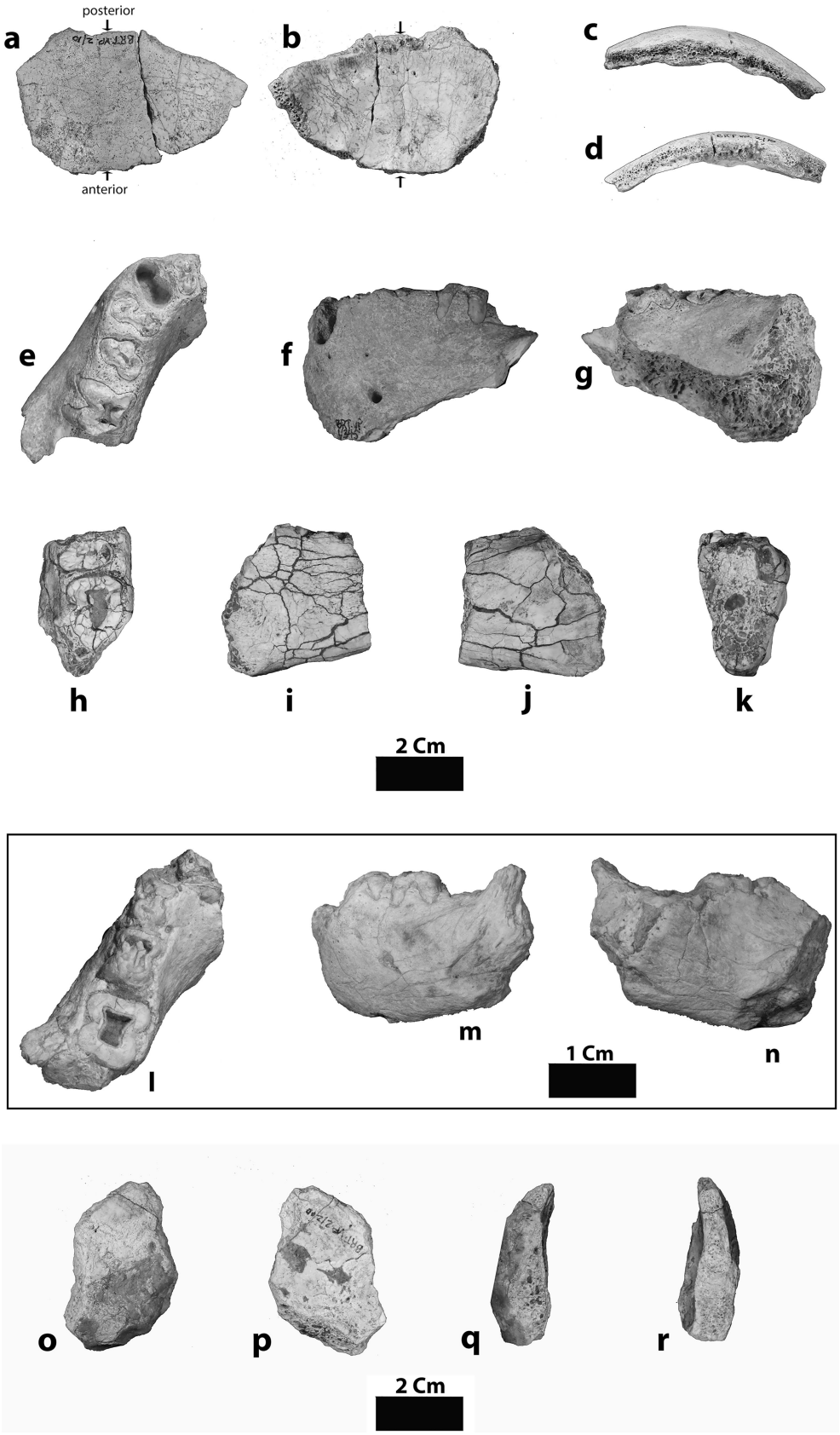


**Extended Data Fig. 2 | Cranial, dental and mandibular specimens from BRT-VP-1 and BRT-VP-2.** BRT-VP-2/10-150 in ectocranial (**a**), endocranial (**b**), anterior (**c**), and posterior (**d**) views. BRT-VP-1/345 in occlusal (**e**), buccal (**f**), and lingual (**g**) views. BRT-VP-1/271 in occlusal (**h**), lingual (**i**), buccal (**j**), and anterior (**k**) views. BRT-VP-2/258 in occlusal (**l**), buccal (**m**), and lingual (**n**) views. BRT-VP-2/200 in ectocranial (**o**), endocranial (**p**), posterior (**q**), and anterior (**r**) views.

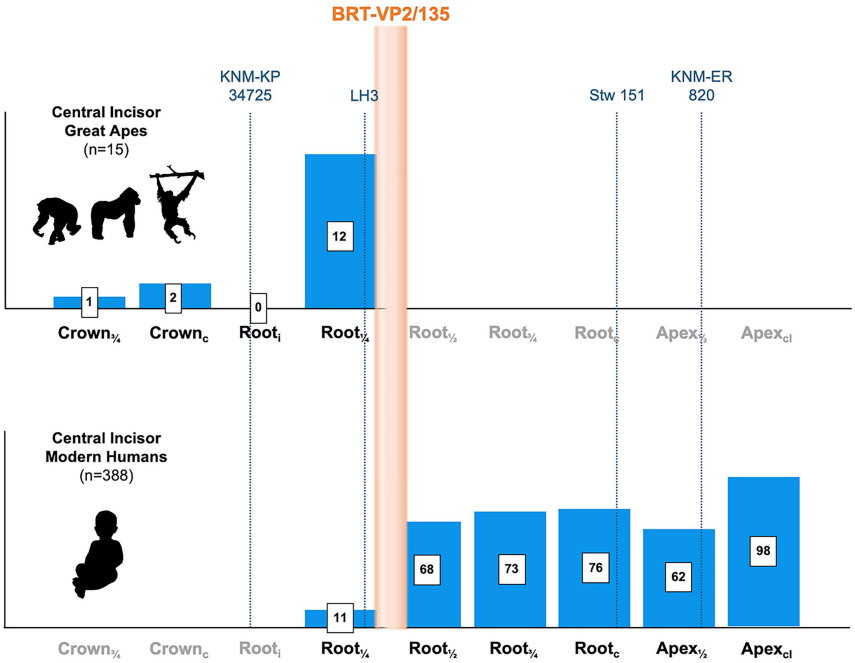


**Extended Data Fig. 3 | Fractional stages of mandibular incisor formation.** This figure (adapted from ref. 22) shows the frequency distribution of the fractional stages of mandibular central incisor (crown & root) formation in extant great ape and modern human individuals where the $M_1$ is at stage $R_{¼}$. Aside from fractional staging, the crown, root, or the root apex of the incisor can be initiating ("i"), complete ("c"), or closed ("cl"). Relative to $M_1$ development, gracile (i.e., chronologically older) australopiths are delayed in incisor formation relative to chronologically younger early *Homo*. Incisor development being at least one half complete (i.e., $R_{½}$ or less) characterizes all great apes and occurs in only 20.4% of all modern humans sampled. Central incisors of BRT-VP2 (orange polygon) are between $R_{¼}$ and $R_{½}$ (slightly closer to $R_{½}$) which, among early hominins that died with their first molar roots three-quarters formed, is most similar to specimens from Laetoli (LH3; *Au. afarensis*) and Kanapoi (KNM-KP 34725; *Au. anamensis*), and dissimilar to early *Homo* (StW 151 and KNM-ER 820). Thus, BRT-VP-2/135 evinces a state of mandibular central incisor development observed in a relatively small fraction of modern humans, but one that is common in great apes. Silhouettes were created using PhyloPic (http://phylopic.org): *Pan troglodytes* by T. M. Keesey under a Creative Commons licence CC BY 3.0; *Gorilla gorilla* by M. Michaud under a Creative Commons licence CCO 1.0; *Pongo* by D. J. Ardesch under a Creative Commons licence CCO 1.0; and *Homo sapiens* by A. Farke under a Creative Commons licence CC BY 3.0.

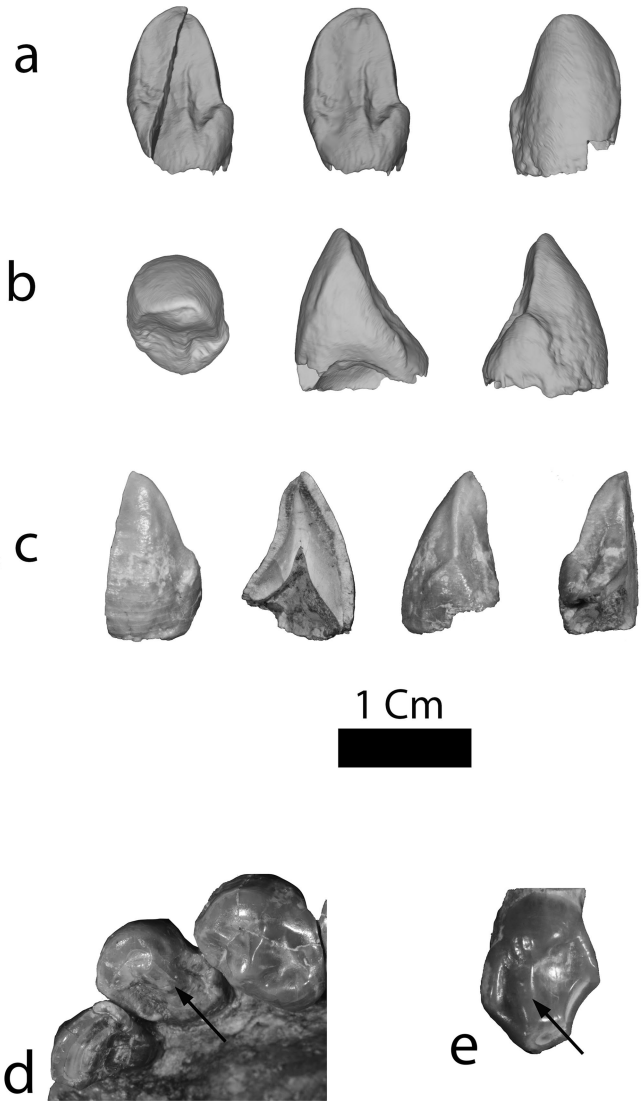


**Extended Data Fig. 4 | BRT-VP-2/135 canines compared to *Au. afarensis* canines. a**, the right canine of BRT-VP-2/135, unreconstructed and reconstructed lingual views, and buccal view. **b**, occlusal, mesial and distal views of the right canine of BRT-VP-2/135. **c**, labial, mesial, distal, and lingual views of the preserved distal half of the left canine of BRT-VP-2/135. **d**, A.L. 400-1b lower canine with prominent vertical lingual ridge (black arrow). **e**, A.L. 200-1 upper canine with prominent vertical lingual ridge. Note that the BRT-VP-2/135 right canine does not have a prominent lingual ridge. Rather, it has a thin crest-like structure that bounds the distal lingual groove mesially.


**Extended Data Fig. 5 | Upper canine crown shape and wear pattern.** Black and grey arrows show the length and orientation of the mesial and distal crown shoulders, respectively. Note that the length and orientation of the mesial crown shoulder in BRT-VP-1/380 is similar to *Au. afarensis*, whereas the distal crown shoulder is short and oriented obliquely as in the *Au. anamensis* canines. The wear pattern in BRT-VP-1/380 is also similar to *Au. anamensis* canines where the wear, as shown by the red stars, extends to the lingual face and basal tubercle of the crown. Figure was adapted from ref. 52, Springer Nature.

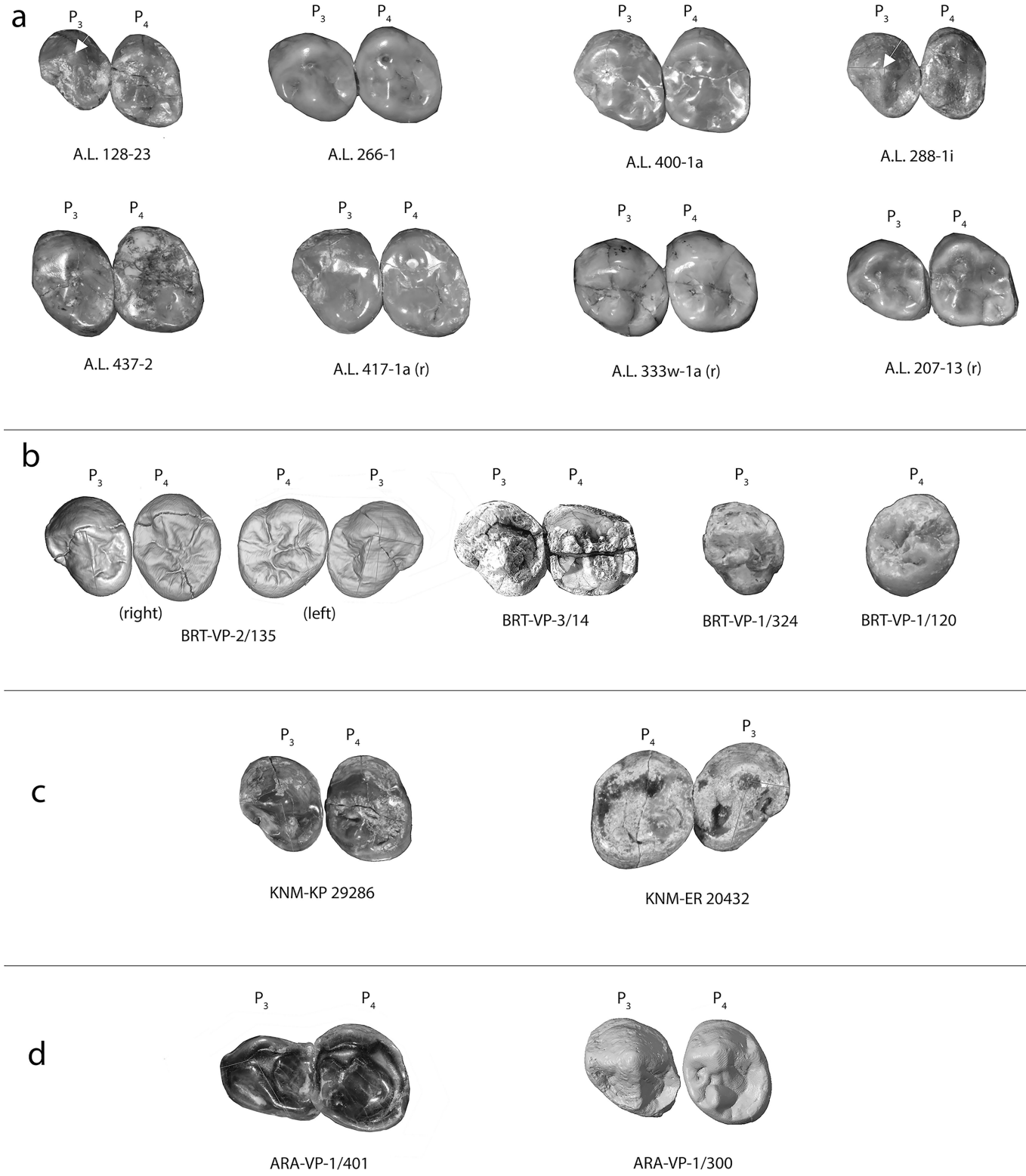


**Extended Data Fig. 6 | Early hominin lower premolar morphology.** Relatively unworn lower premolars of *Au. afarensis* (**a**), BRT-VP-2/135 (**b**), *Au. anamensis* (**c**), and *Ar. ramidus* (**d**). Some $P_3$s of *Au. afarensis* have more primitive occlusal morphology (e.g., metaconid non-existent or incipient, centrally positioned protoconid (white arrow)). However, like the derived $P_3$s with well-developed metaconid, they are associated with a $P_4$ that has a rhomboidal occlusal outline. The mesial protoconid crest-transverse crest angle is <90° as shown in A.L. 128-23 and A.L. 288-1i. On the other hand, The $P_3$s of BRT-VP-2/135 (**b**), have diminutive to absent metaconid with a centrally positioned protoconid and the mesial protoconid crest-transverse crest angle is >90°. The $P_4$s are also oval in occlusal outline. This is the combination of traits seen in the earlier hominins such as *Au. anamensis* (c) and *Ar. ramidus* (d).

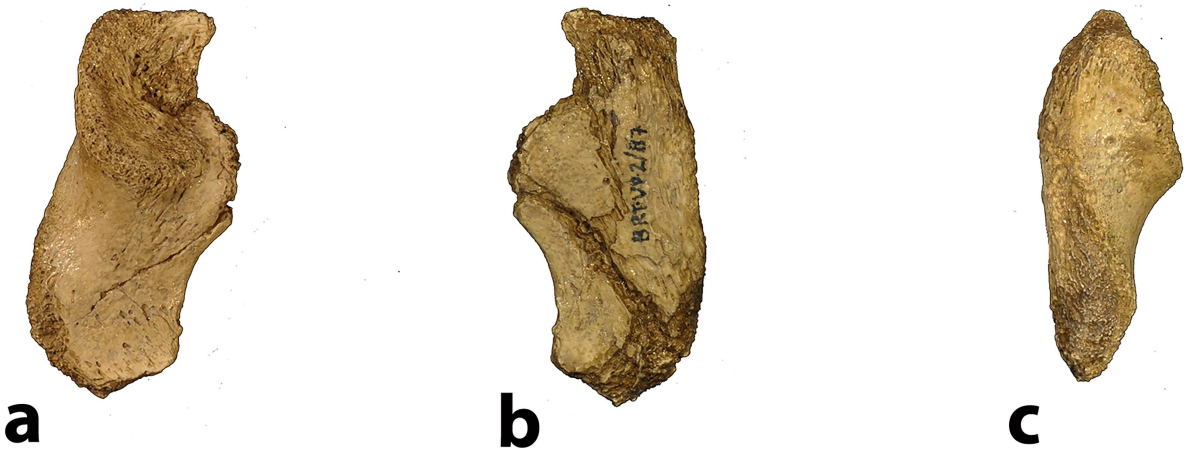


**Extended Data Fig. 7 | BRT-VP-2/87.** Lateral (**a**), medial (**b**), and posterior (**c**) views.


**Extended Data Fig. 8 | Ontogenetic series of juvenile human ischia.** Fourteen modern human ischia ranging in age from 1 to 6 years are shown. The age and sex of each individual are provided. y = year; (M) = male; (F) = female. These specimens were sampled from the Hamann-Todd human skeletal collection at the Cleveland Museum of Natural History, Cleveland, OH, USA.

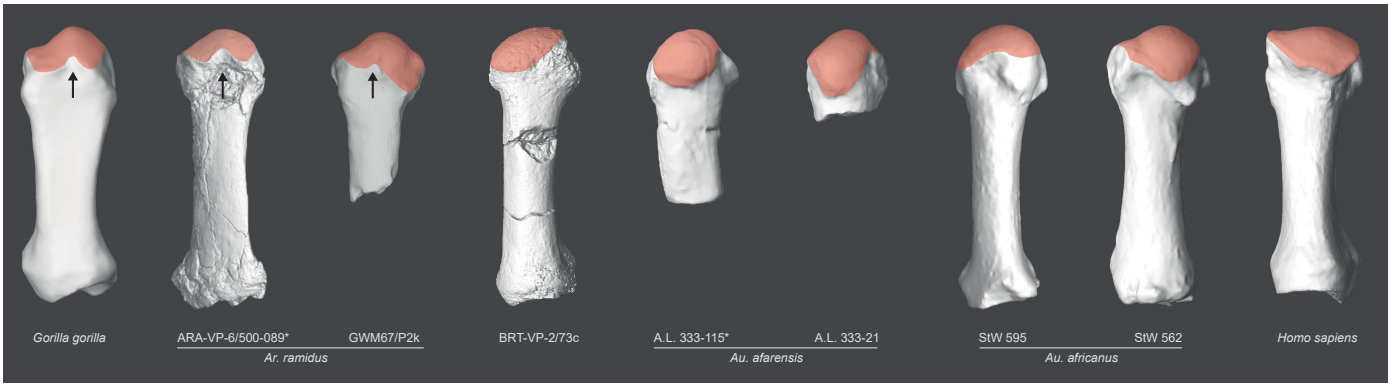


**Extended Data Fig. 9 | Hallucal metatarsophalangeal joint morphology in early hominins.** Note the presence of a nonsubchondral isthmus in *Gorilla gorilla* and *Ardipithecus ramidus* (ARA-VP-6/500-089, GWM67/P2k). In contrast, BRT-VP-2/73c, A.L. 333-115, and A.L. 333-21, StW 562, and StW 595 possess more rounded articular facets, which is the condition derived toward later hominins. Note that StW 562 and StW 595 have bony growths on the dorsolateral region of the head, which are non-articular and do not contribute to the formation of a nonsubchondral isthmus. Also note the extreme dorsal head doming of AL. 333-115 and A.L. 333-21 compared to the *Homo sapiens* MT1. The asterisk signifies the specimen was mirrored for comparison to BRT-VP-2/73c. The ARA-VP-6/500-089 image was reproduced from ref. 34, AAAS. The GWM67/P2k image was provided by S. W. Simpson. All other scans were generated by T.C.P.

nature portfolio

Corresponding author(s): Yohannes Haile-Selassie

Last updated by author(s): September 4, 2025

# Reporting Summary

Nature Portfolio wishes to improve the reproducibility of the work that we publish. This form provides structure for consistency and transparency in reporting. For further information on Nature Portfolio policies, see our Editorial Policies and the Editorial Policy Checklist.

Please do not complete any field with "not applicable" or n/a. Refer to the help text for what text to use if an item is not relevant to your study.
For final submission: please carefully check your responses for accuracy; you will not be able to make changes later.

## Statistics

For all statistical analyses, confirm that the following items are present in the figure legend, table legend, main text, or Methods section.

| n/a | Confirmed | |
|---|---|---|
| ☐ | ■ | The exact sample size (*n*) for each experimental group/condition, given as a discrete number and unit of measurement |
| ☐ | ☐ | A statement on whether measurements were taken from distinct samples or whether the same sample was measured repeatedly |
| ☐ | ☐ | The statistical test(s) used AND whether they are one- or two-sided<br>*Only common tests should be described solely by name; describe more complex techniques in the Methods section.* |
| ☐ | ☐ | A description of all covariates tested |
| ☐ | ☐ | A description of any assumptions or corrections, such as tests of normality and adjustment for multiple comparisons |
| ☐ | ☐ | A full description of the statistical parameters including central tendency (e.g. means) or other basic estimates (e.g. regression coefficient) AND variation (e.g. standard deviation) or associated estimates of uncertainty (e.g. confidence intervals) |
| ☐ | ☐ | For null hypothesis testing, the test statistic (e.g. *F*, *t*, *r*) with confidence intervals, effect sizes, degrees of freedom and *P* value noted<br>*Give P values as exact values whenever suitable.* |
| ☐ | ☐ | For Bayesian analysis, information on the choice of priors and Markov chain Monte Carlo settings |
| ☐ | ☐ | For hierarchical and complex designs, identification of the appropriate level for tests and full reporting of outcomes |
| ☐ | ☐ | Estimates of effect sizes (e.g. Cohen's *d*, Pearson's *r*), indicating how they were calculated |

*Our web collection on statistics for biologists contains articles on many of the points above.*

## Software and code

Policy information about availability of computer code

| | |
|---|---|
| Data collection | All dental and mandibular measurements were taken using Mitutoyo digital caliper. |
| Data analysis | Avizo v.9.5 (ThermoFisher Scientific Inc., Waltham, MA, USA) was used for 3D rendering of study specimens; GeoMagic Wrap 2017 (Artec 3D, Senningerberg, Luxembourg) for surface model processing; Thermo Fisher MAT 253 MS (ThermoFisher Scientific Inc., Waltham, MA, USA) for isotope analysis; R Statistics (2024.04.2 |

For manuscripts utilizing custom algorithms or software that are central to the research but not yet described in published literature, software must be made available to editors and reviewers. We strongly encourage code deposition in a community repository (e.g. GitHub). See the Nature Portfolio guidelines for submitting code & software for further information.

## Data

Policy information about availability of data

All manuscripts must include a data availability statement. This statement should provide the following information, where applicable:

- Accession codes, unique identifiers, or web links for publicly available datasets
- A description of any restrictions on data availability
- For clinical datasets or third party data, please ensure that the statement adheres to our policy

All data presented in this manuscript and Extended Data Tables 1 and 2 are publicly accessible. Request to access 3D scans of specimens included in this manuscript should be sent to the

## Research involving human participants, their data, or biological material

Policy information about studies with human participants or human data. See also policy information about sex, gender (identity/presentation), and sexual orientation and race, ethnicity and racism.

| | |
|---|---|
| Reporting on sex and gender | |
| Reporting on race, ethnicity, or other socially relevant groupings | |
| Population characteristics | |
| Recruitment | |
| Ethics oversight | |

Note that full information on the approval of the study protocol must also be provided in the manuscript.

# Field-specific reporting

Please select the one below that is the best fit for your research. If you are not sure, read the appropriate sections before making your selection.

☐ Life sciences ☐ Behavioural & social sciences ■ Ecological, evolutionary & environmental sciences

For a reference copy of the document with all sections, see nature.com/documents/nr-reporting-summary-flat.pdf

# Life sciences study design

All studies must disclose on these points even when the disclosure is negative.

| | |
|---|---|
| Sample size | |
| Data exclusions | |
| Replication | |
| Randomization | |
| Blinding | |

# Behavioural & social sciences study design

All studies must disclose on these points even when the disclosure is negative.

| | |
|---|---|
| Study description | |
| Research sample | |
| Sampling strategy | |
| Data collection | |
| Timing | |
| Data exclusions | |
| Non-participation | |
| Randomization | |

# Ecological, evolutionary & environmental sciences study design

All studies must disclose on these points even when the disclosure is negative.

| | |
|---|---|
| Study description | We describe and assess the taxonomic affinity of newly recovered hominin fossils from Woranso-Mille, Afar Region, Ethiopia, and address diet and locomotion in Australopithecus deyiremeda. |
| Research sample | Dentognathic hominin fossils from the mid-Pliocene of Woranso-Mille and other eastern and South African sites. |
| Sampling strategy | Fieldwork was conducted at Woranso-Mille site in Ethiopia to collect the hominin fossils described here. |
| Data collection | Primary geological and palaeontological data for Woranso-Mille hominins were collected by the authors in the field and laboratory. Comparative data was collected from previously published resources. |
| Timing and spatial scale | N/A |
| Data exclusions | No available data relevant to the study were excluded. |
| Reproducibility | Dentognathic measurements taken by the authors are reproducible because they were taken using standard methods used by researchers in paleontology. |
| Randomization | Randomization was not used in this study because none of the comparative descriptions presented here required randomization. |
| Blinding | Not used in this study. |

Did the study involve field work? ■ Yes ☐ No

## Field work, collection and transport

| | |
|---|---|
| Field conditions | There were no obstructions in our fossil collection in the field. |
| Location | Woranso-Mille palaeontological site is located in the Afar region of Ethiopia. |
| Access & import/export | The Ethiopian Heritage Authority and the Ministry of Mines of the Ethiopian government issue permits to export geological samples from Ethiopia to the United States and Europe for dating and paleomagnetic analyses. Access to fossils in the laboratory is facilitated by the Ethiopian Heritage Authority. |
| Disturbance | None. |

# Reporting for specific materials, systems and methods

We require information from authors about some types of materials, experimental systems and methods used in many studies. Here, indicate whether each material, system or method listed is relevant to your study. If you are not sure if a list item applies to your research, read the appropriate section before selecting a response.

### Materials & experimental systems

| n/a | Involved in the study |
|---|---|
| ☐ | ☐ Antibodies |
| ☐ | ☐ Eukaryotic cell lines |
| ☐ | ■ Palaeontology and archaeology |
| ☐ | ☐ Animals and other organisms |
| ☐ | ☐ Clinical data |
| ☐ | ☐ Dual use research of concern |
| ☐ | ☐ Plants |

### Methods

| n/a | Involved in the study |
|---|---|
| ☐ | ☐ ChIP-seq |
| ☐ | ☐ Flow cytometry |
| ☐ | ☐ MRI-based neuroimaging |

## Antibodies

| | |
|---|---|
| Antibodies used | |
| Validation | |

## Eukaryotic cell lines

Policy information about cell lines and Sex and Gender in Research

| | |
|---|---|
| Cell line source(s) | |
| Authentication | |
| Mycoplasma contamination | |
| Commonly misidentified lines (See ICLAC register) | |

## Palaeontology and Archaeology

| | |
|---|---|
| Specimen provenance | The hominin fossils described in this study were collected from Pliocene exposures at Woranso-Mille palaeontological site located in the Afar region of Ethiopia. |
| Specimen deposition | All fossils are housed in the palaeoanthropology Laboratory of the National Museum of Ethiopia and can be accessed by other researchers who comply with Ethiopian antiquities laws |
| Dating methods | Geological age of the hominins was determined by dating volcanogenic rocks using the Ar/Ar method and additional paleomagnetic data. Detailed information is provided in the Supplementary Information |

■ Tick this box to confirm that the raw and calibrated dates are available in the paper or in Supplementary Information.

| | |
|---|---|
| Ethics oversight | Woranso-Mille project conducts its field and laboratory research through permits issued by the Ethiopian Heritage Authority and the Afar Regional Government. The Ethiopian Heritage Authority and the Ministry of Mines of the Ethiopian government issue permits to export geological samples from Ethiopia to the United |

Note that full information on the approval of the study protocol must also be provided in the manuscript.

## Animals and other research organisms

Policy information about studies involving animals; ARRIVE guidelines recommended for reporting animal research, and Sex and Gender in Research

| | |
|---|---|
| Laboratory animals | |
| Wild animals | |
| Reporting on sex | |
| Field-collected samples | |
| Ethics oversight | |

Note that full information on the approval of the study protocol must also be provided in the manuscript.

## Clinical data

Policy information about clinical studies

All manuscripts should comply with the ICMJE guidelines for publication of clinical research and a completed CONSORT checklist must be included with all submissions.

| | |
|---|---|
| Clinical trial registration | |
| Study protocol | |
| Data collection | |
| Outcomes | |

## Dual use research of concern

Policy information about dual use research of concern

### Hazards

Could the accidental, deliberate or reckless misuse of agents or technologies generated in the work, or the application of information presented in the manuscript, pose a threat to:

| No | Yes | |
|---|---|---|
| ☐ | ☐ | Public health |
| ☐ | ☐ | National security |
| ☐ | ☐ | Crops and/or livestock |
| ☐ | ☐ | Ecosystems |
| ☐ | ☐ | Any other significant area |

### Experiments of concern

Does the work involve any of these experiments of concern:

| No | Yes | |
|---|---|---|
| ☐ | ☐ | Demonstrate how to render a vaccine ineffective |
| ☐ | ☐ | Confer resistance to therapeutically useful antibiotics or antiviral agents |
| ☐ | ☐ | Enhance the virulence of a pathogen or render a nonpathogen virulent |
| ☐ | ☐ | Increase transmissibility of a pathogen |
| ☐ | ☐ | Alter the host range of a pathogen |
| ☐ | ☐ | Enable evasion of diagnostic/detection modalities |
| ☐ | ☐ | Enable the weaponization of a biological agent or toxin |
| ☐ | ☐ | Any other potentially harmful combination of experiments and agents |

## Plants

Seed stocks

Novel plant genotypes

Authentication

## ChIP-seq

### Data deposition

☐ Confirm that both raw and final processed data have been deposited in a public database such as GEO.

☐ Confirm that you have deposited or provided access to graph files (e.g. BED files) for the called peaks.

Data access links
*May remain private before publication.*

Files in database submission

Genome browser session
(e.g. UCSC)

### Methodology

Replicates

Sequencing depth

Antibodies

Peak calling parameters

Data quality

Software

## Flow Cytometry

### Plots

Confirm that:

☐ The axis labels state the marker and fluorochrome used (e.g. CD4-FITC).

☐ The axis scales are clearly visible. Include numbers along axes only for bottom left plot of group (a 'group' is an analysis of identical markers).

☐ All plots are contour plots with outliers or pseudocolor plots.

☐ A numerical value for number of cells or percentage (with statistics) is provided.

### Methodology

Sample preparation

Instrument

Software

Cell population abundance

Gating strategy

☐ Tick this box to confirm that a figure exemplifying the gating strategy is provided in the Supplementary Information.

## Magnetic resonance imaging

### Experimental design

Design type

Design specifications

Behavioral performance measures

Imaging type(s)

Field strength

Sequence & imaging parameters

Area of acquisition

Diffusion MRI ☐ Used ☐ Not used

### Preprocessing

Preprocessing software

Normalization

Normalization template

Noise and artifact removal

Volume censoring

### Statistical modeling & inference

Model type and settings

Effect(s) tested

Specify type of analysis: ☐ Whole brain ☐ ROI-based ☐ Both

Statistic type for inference

(See Eklund et al. 2016)

Correction

## Models & analysis

| n/a | Involved in the study |
|---|---|
| ☐ | ☐ Functional and/or effective connectivity |
| ☐ | ☐ Graph analysis |
| ☐ | ☐ Multivariate modeling or predictive analysis |

Functional and/or effective connectivity

Graph analysis

Multivariate modeling and predictive analysis